9. SITE 755[1]

Shipboard Scientific Party[2]

HOLE 755A

Date occupied: 22 May 1988

Date departed: 24 May 1988

Time on hole: 1 day, 16 hr, 16 min

Position: 31°01.786'S, 93°32.803'E

Bottom felt (rig floor; m; drill-pipe measurement): 1068.8

Distance between rig floor and sea level (m): 10.87

Water depth (drill-pipe measurement; corrected m): 1057.9

Total depth (rig floor; corrected m): 1277.2

Penetration (m): 208.4

Number of cores: 19

Total length of cored section (m): 178.4

Total core recovered (m): 80.21

Core recovery (%): 44

Oldest sediment cored:
Depth sub-bottom (m): 208.4
Nature: calcareous vitric tuff
Earliest age: Turonian
Measured velocity (km/s): 2.5–3.0

Principal results: Site 755 (proposed Site BR-4) was drilled about 4 km north of the south-facing escarpment of Broken Ridge in order to sample the basal part of the dipping and truncated sedimentary section. The main drilling objective was to penetrate and sample a particularly prominent seismic reflector that outcrops at the tip of Broken Ridge and lies 0.180 s two-way traveltime (TWT) below seafloor (bsf) at Site 755. Owing to time constraints, however, drilling at Site 755 was terminated after penetrating 208 m below seafloor (mbsf), slightly above the estimated level of the target reflector.

The site is at shotpoint 1237 on line 20 of the seismic survey conducted by Cruise 2708 of *Robert D. Conrad* (RC2708). The actual site location was chosen to avoid a buried talus deposit, which was probably eroded from the tip of the ridge, evident in the 3.5-kHz echo-sounder profiles made prior to site occupation. The basal part of the dipping and truncated sequence is unconformably overlain by about 60 m (0.08 s TWT bsf) of subhorizontally layered Neogene ooze.

Site 755 consists of only one hole, Hole 755A. After punching a mud-line core and washing to 36 mbsf, Hole 755A was cored with the rotary core barrel (RCB) to a total depth of 208 mbsf before drilling was terminated. As at Sites 752 and 754, the layer containing detrital sand, gravel, and shelly material immediately above the erosional unconformity proved difficult to recover (about 2% recovery in the interval from 36 to 65 mbsf). The Neogene/Cretaceous unconformity was penetrated at about 65.5 mbsf.

Two lithologic units are recognized at Site 755:

Unit I (0–65.5 mbsf): Pleistocene to middle Miocene foraminifer nannofossil ooze and nannofossil ooze with foraminifers. Sediment color varies from light gray in the uppermost part to white through most of the unit and grades into a pale brown toward the base. White and pale brown mottles occur throughout. The base of Unit I is defined by a layer of fossiliferous shelly foraminifer grainstone. Recovered fragments are dark yellow brown to white in color, with some stained rusty red from oxidized iron.

Unit II (65.5–208.4 mbsf): Santonian to Turonian tuff containing varying amounts of micrite, glauconite, and ashy limestone (in the upper part). Unit II is divided into three subunits:

Subunit IIA (65.5–140.8 mbsf): Santonian to Coniacian-Turonian tuff (50%–90% volcanic ash) with interbedded ashy limestone. The uppermost 2.5 m of ashy limestone is iron stained along bedding planes and fractures, and the degree of staining decreases with depth over the interval.

Subunit IIB (140.8–189 mbsf): Coniacian to Turonian tuff (40%–80% ash) containing glauconite that decreases in abundance downsection. The glauconite grains are large and granular, up to coarse sand size. A 2–3-cm-thick gypsum layer fills a fracture at 151.7 mbsf.

Subunit IIC (189–208.4 mbsf): Coniacian to Turonian tuffs (60%–90% ash) with varying amounts of micrite. The coarse-grained, glauconite-rich layers in the upper 10 m of this subunit have sharp basal contacts and fine upward. Light gray to dark greenish gray mottling is more pronounced away from these coarse sand intervals. Some microfractures and vugs are filled with secondary and authigenic minerals, calcite, gypsum, and pyrite. Three nodules of recrystallized sparry calcite occur in the basal 10 m of the subunit.

The carbonate content of the Upper Cretaceous sediments at Site 755 is significantly lower than in younger parts of the dipping and truncated sequence drilled at the other Broken Ridge sites. Carbonate content increases upsection from an average of 10% in the Turonian to about 30% in the lower Santonian sediments. The mean accumulation rate for volcanic ash for the same interval decreases from about 9 to 3 g/cm^2/1000 yr. A significant change in sedimentation on Broken Ridge apparently took place between deposition of the Turonian to Santonian tuffs sampled at Site 755 and the Maestrichtian limestones found at Site 754. Biological productivity increased markedly over the intervening and unsampled 10 m.y., while ash accumulation, and hence nearby eruptive activity, waned (see the following discussion).

Discussions aboard ship focused on the significance of the recrystallized calcite nodules in the tuffs immediately above the prominent seismic reflector on RC2708 seismic-reflection line 20. Because compressional-wave velocity in these nodules is high (~4100 m/s), whereas velocities in the primarily tuffaceous lithologies drilled between 160 and 208 mbsf at Site 755 are considerably lower (~2600 m/s), a lithologic change downsection from tuff to completely recrystallized limestone could possibly produce the strong reflections observed in the seismic data.

Depths of deposition at Site 755 were outer shelf/upper slope during the Turonian to Santonian, according to planktonic/benthic foraminifer ratios. Benthic foraminifer assemblages, however, indicate deposition in slightly deeper water (middle to upper bathyal) during that time interval. According to benthic foraminifer studies of sediments in the dipping, truncated section at Broken Ridge, depositional depths appear to have been in the range of 200–600 m during the Late Cretaceous and early Paleogene, deepening to middle to lower bathyal depths by the middle Eocene. Above the angular unconformity, depositional depths in the Neogene were middle bathyal, about the same depth as at present. However, a reworked assemblage of mollusks, bryozoans, and coral fragments which is indicative of a shallow-water environment was found mixed with deeper water oozes in a sample from 45 to 56 mbsf, the interval above the unconformity where recovery was extremely poor.

[1] Peirce, J., Weissel, J., et al., 1989. *Proc. ODP, Init. Repts.*, 121: College Station, TX (Ocean Drilling Program).

[2] Shipboard Scientific Party is as given in the list of Participants preceding the contents.

Remanent magnetization measurements at Site 755 show that all sediments recovered from below the angular unconformity are normally magnetized, as expected for the Turonian to Santonian age range obtained from the micropaleontology. Susceptibility measurements from these Upper Cretaceous samples are used as a guide to volcanic ash content in the section. If valid, this approach suggests increasing volcanic activity from the bottom of the cored section (208 mbsf) to a paroxysmal eruptive phase recorded at 190 mbsf. The ash content suggests that activity waned gradually upsection to about 150 mbsf, followed by more sporadic eruptive phases of either lesser magnitude or possibly occurring at greater distances from Site 755.

Microscopic examination of polished thin sections revealed traces of terrestrial organic matter (inertinite and vitrinite) in the Turonian to lower Santonian sediments at Site 755 (see "Organic Geochemistry" section of the "Broken Ridge Summary," this volume). These fragments are up to 50 μm in size, suggesting that the plant particles were not transported a great distance from their land source area. In addition, apatite grains (probably authigenic) are found in smear slides of volcanic ashes from Sites 752, 754, and 755 on Broken Ridge. Shorebased studies could therefore include apatite fission track analysis for either additional age dating in the relatively unfossiliferous tuffs at Site 755 or thermal history studies of the sedimentary section at Broken Ridge.

BACKGROUND AND OBJECTIVES

Overview

Detailed discussions of the background and objectives for drilling at Broken Ridge during ODP Leg 121 are found in the "Leg 121 Background and Objectives" chapter and in the "Background and Objectives" section of the "Site 752" chapter (this volume). The reader is referred there for general information. The particular drilling objectives for Site 755 (Fig. 1) are described in this section.

Drilling Objectives for Site 755

Site 755 (proposed Site BR-4) is 4 km north of the south-facing escarpment of Broken Ridge, at the southern end of a north-south transect of drill sites across the crest of the ridge (Fig. 1). This transect of four drill sites was intended to sample the entire dipping and truncated sedimentary sequence at Broken Ridge in single-bit holes, each placed to provide overlap of section between sites. Because of time constraints and mechanical difficulties with coring at Sites 753 and 754 (proposed Sites BR-1 and BR-3, respectively), only Sites 752 (proposed Site BR-2) and 754 achieved the goal of stratigraphic overlap. About 450 m of the dipping and truncated sequence remains undrilled between the bottom of Hole 754B and the top of that sequence at Site 755.

Site 755 was situated to penetrate and sample the basal part of the dipping and truncated sedimentary sequence at Broken Ridge (Fig. 2). This basal section is unconformably overlain by about 65 m of subhorizontally layered Neogene ooze. Based on seismic-reflector correlation from the location of Deep Sea Drilling Project (DSDP) Site 255 (Fig. 1), the dipping and truncated section at Site 755 would be stratigraphically lower than the limestones and cherts of Santonian age drilled at Site 255 (see "Broken Ridge Underway Geophysics" chapter, this volume).

The principal objective at Site 755 was to ascertain the age, lithology, and depth of deposition of the sediments in the basal part of the dipping and truncated sequence at Broken Ridge for comparison with the stratigraphically higher units in that sequence sampled at Sites 752 through 754. That objective was achieved. The planned depth of penetration at Site 755 called for drilling through a particularly prominent seismic reflector at 0.180 s TWT bsf that outcrops above the main south-facing escarpment of Broken Ridge (Fig. 2). Because of time constraints, however, drilling at Site 755 was terminated at a depth of 208 mbsf, still above the target reflector. Thus, our second objective at Site 755, of determining the cause for the strong reflector and its implications, was not met.

OPERATIONS

Site 755

We conducted a short 3.5-kHz echo-sounder survey to assure that the location of Site 755 would be positioned to avoid what was interpreted from the general survey of Broken Ridge as possible talus rubble. The final site position was selected to be just north of the talus pile, where only a thin sediment cover capped the underlying dipping sediments. The coring objective at Site 755 was to achieve maximum penetration in the 36 hr remaining for operations at Broken Ridge. The short move from Sites 752 to 755 was made in 2.5 hr, and the beacon was dropped at 1448 hr (local time), 22 May 1988.

Hole 755A

The drill pipe was lowered to the seafloor with the RCB bottom-hole assembly and a new C-4 type 9$^7/_8$" roller-cone bit. A routine mud-line punch core established the water depth to be 1068.8 m below rig floor, as measured by the drill pipe. Because Site 755 is within 12 nmi of the other Broken Ridge sites and because the Neogene cap was sampled at each of the other sites, the bit was washed ahead to 36.1 mbsf before coring resumed. The elusive band of beach-type sand, gravel, and shell fragments that had frustrated coring attempts at the previous three sites again proved nearly impossible to recover. Below the Neogene/Cretaceous unconformity the formation changed to a tough limestone with abundant ash and some chert, which drilled with unusual difficulty; some 9.7-m intervals required over 90 min to cut. Recovery and drilling time varied with the differing hard constituents encountered in the softer volcanogenic material. When the allotted time for this site expired, the final Core 121-755A-19R was retrieved and the hole was abandoned. Total penetration was 208.4 mbsf (Table 1). The pipe was pulled out of the hole, and the bit was on deck at 0715 hr, 24 May. Time on site was 40.25 hr, with 45% core recovery. The ship was underway for Ninetyeast Ridge from the last Leg 121 drill site on Broken Ridge at 0730 hr.

LITHOSTRATIGRAPHY AND SEDIMENTOLOGY

Sediments of Pleistocene through Cretaceous age were recovered at Site 755 before drilling was terminated in Turonian tuff. The two sedimentary units in Hole 755A are Unit I, 65.5 m of foraminifer nannofossil ooze and nannofossil ooze with foraminifers of Pleistocene to middle Miocene age, and Unit II, 143 m of tuff with varying amounts of glauconite and micrite and of Santonian to Turonian age (Table 2 and Fig. 3).

Unit I (Cores 121-755A-1R to 121-755A-5R; 0–65.5 mbsf, with only 12% recovery) is dominated by a nannofossil ooze with varying amounts of foraminifers. The color varies with depth, grading from light gray (10YR 7/2) in the top of Core 121-755A-1R, to white (10YR 8/2) in the middle of the unit, to a very pale brown (10YR 8/3 and 10YR 7/3) toward the base of Core 121-755A-1R. White (10YR 8/2) and pale brown (10YR 6/3) mottles occur throughout. Core 121-755A-3R recovered 60 cm of disturbed white (10YR 8/2) foraminifer nannofossil ooze. Shell fragments (gastropod and pteropod shells, bryozoans, brachiopods, and corals) occur in Section 121-755A-3R-CC.

The base of Unit I is defined by a layer of fossiliferous shelly foraminifer grainstone, similar to coquina (Fig. 4). The color ranges from a dark yellow brown (10YR 3/4) to white (10YR 8/2). Parts of the shelly foraminifer grainstone are stained a rusty red color by oxidized iron. A bivalve mold, 0.5 cm long, occurs within this layer. A sharp contact between drilling bis-

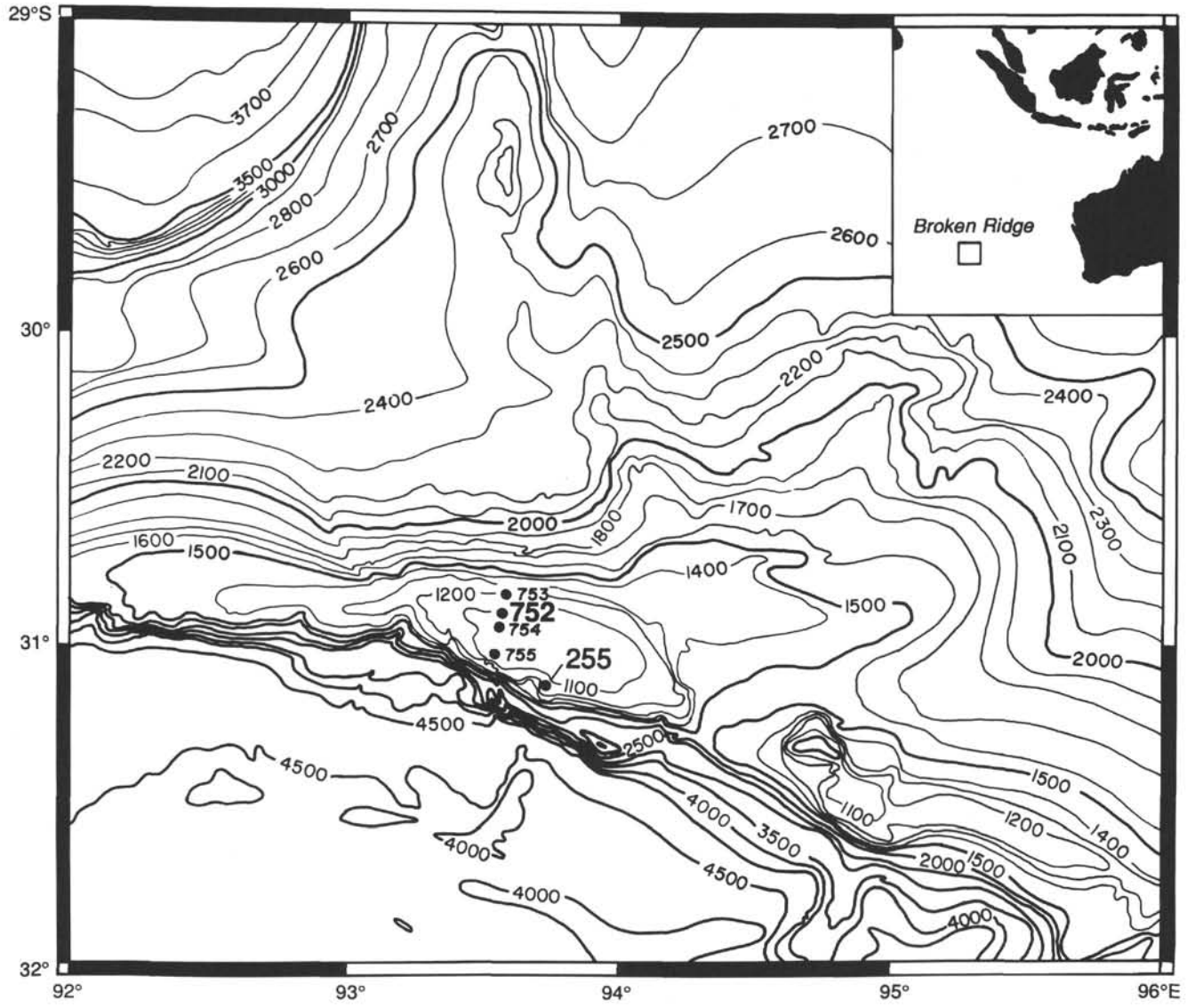

Figure 1. Bathymetric map showing locations of ODP Site 755, DSDP Site 255, and other Leg 121 sites at Broken Ridge. Bathymetry, which is based mainly on RC2708 echo-sounder data, is contoured at 100-m intervals except along the south-facing escarpment, where contours are omitted for clarity.

cuits separates the shelly foraminifer grainstone from the underlying tuffs with interbedded intervals of ashy limestone (Fig. 3).

Unit II (Cores 121-755A-5R to 121-755A-19R; 65.5–208.4 mbsf) consists of upper Santonian to Turonian tuff with varying amounts of micrite and glauconite. Unit II is divided into three subunits (Table 2): Subunit IIA (Cores 121-755A-5R to 121-755A-12R; 65.5–140.8 mbsf) is a tuff with varying amounts of micrite and intervals of ashy limestone interspersed within the tuffs in the top of the subunit, Subunit IIB (Cores 121-755A-13R to 121-755A-17R; 140.8–189.0 mbsf) is a tuff with varying amounts of glauconite, and Subunit IIC (Cores 121-755A-18R to 121-755A-19R; 189.0–208.4 mbsf) contains tuff with varying amounts of micrite.

Subunit IIA is capped by a tuff with intervals of ashy limestone interspersed in Cores 121-755A-5R to 121-755A-6R (65.5–81.8 mbsf). The ashy limestone (30%–40% ash) is an olive (5Y 5/6 to 5Y 5/4) color, with iron staining concentrated in small fractures and bedding planes in Sections 121-755A-5R-1 and 121-755A-5R-2. The iron staining gradually decreases with depth within this interval. Sand-sized grains, predominantly volcanic glass and trace amounts of glauconite, and *Inoceramus* shell fragments occur throughout the ashy limestone. A color change to dark greenish gray (5BG 4/1) delineates the lithologic boundary between the ashy limestones and the tuffs. The tuffs (50%–90% ash) are weakly laminated, and some bedding planes separate layers of different grain size. Slight to moderate mottling of the tuffs is visible. *Inoceramus* shell fragments and black flecks of volcanic glass occur throughout. The amount of micrite diminishes downcore. Alternating zones of greenish gray (5GY 5/1) to dark greenish (5GY 5/1) and light greenish gray (5G 7/1) to grayish olive green (5GY 3/2) tuff with micrite occur in Cores 121-755A-7R to 121-755A-12R (81.8–140.8 mbsf). The greenish gray (5G 7/1) to dark greenish (5GY 5/1) intervals are more strongly bioturbated and mottled, with dark sand-sized particles of glauconite within the mottles. The dark greenish (5GY 5/1) glauconite-rich intervals have fairly sharp lower contacts. Small fractures and vugs are filled with secondary minerals, calcite, and pyrite. Shell fragments occur throughout Core 121-755A-10R, along with several 1-cm-thick zones of concentrated shell fragments. Thin layers of greenish gray (5GY 6/1)

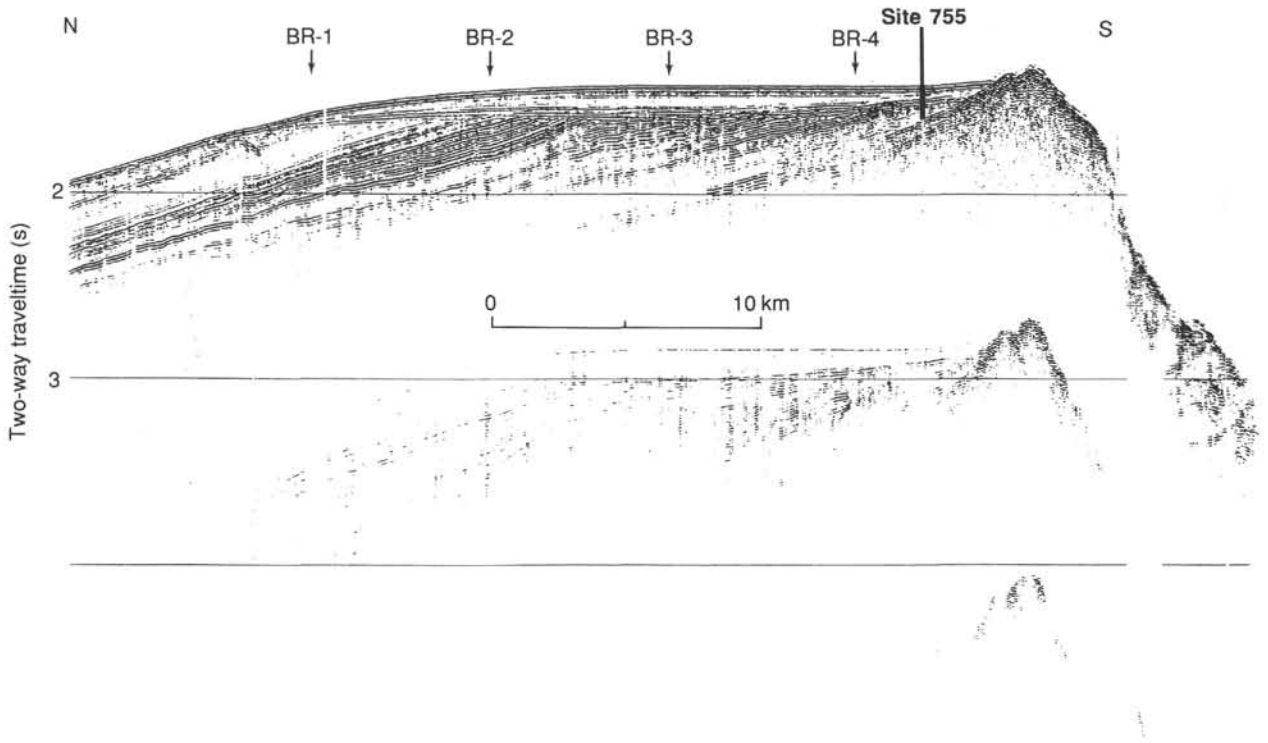

Figure 2. RC2708 single-channel seismic-reflection profile line 20 across Broken Ridge showing the location of Site 755 and proposed Sites BR-1 to BR-4.

Table 1. Coring summary, Site 755.

Core no.	Date (May 1988)	Time (local)	Depth top (mbsf)	Depth bottom (mbsf)	Length cored (m)	Length recovered (m)	Recovery (%)
1R	22	1910	0.0	7.1	7.1	7.10	100.0
2R	22	2020	36.1	45.8	9.7	0.00	0.0
3R	22	2100	45.8	55.5	9.7	0.65	6.7
4R	22	2125	55.5	65.2	9.7	0.00	0.0
5R	22	2245	65.2	72.1	6.9	2.84	41.1
6R	23	0125	72.1	81.8	9.7	5.41	55.8
7R	23	0335	81.8	91.5	9.7	2.93	30.2
8R	23	0515	91.5	101.2	9.7	0.61	6.3
9R	23	0650	101.2	110.9	9.7	2.82	29.1
10R	23	0845	110.9	120.5	9.6	3.28	34.1
11R	23	1110	120.5	130.1	9.6	0.88	9.2
12R	23	1414	131.1	140.8	9.7	1.31	13.5
13R	23	1610	140.8	150.4	9.6	5.02	52.3
14R	23	1805	150.4	160.0	9.6	5.68	59.1
15R	23	1930	160.0	169.7	9.7	8.38	86.4
16R	23	2110	169.7	179.3	9.6	8.58	89.4
17R	23	2310	179.3	189.0	9.7	4.81	49.6
18R	24	0125	189.0	198.7	9.7	9.97	103.0
19R	24	0340	198.7	208.4	9.7	9.94	102.0
					178.4	80.21	45.0

porcellanite, with small fragments of chert, occur in Cores 121-755A-7R and 121-755A-8R.

Subunit IIB consists of a tuff (40%–80% ash) with varying amounts of glauconite; the abundance of the glauconite diminishes downcore in this subunit. Zones of dark blue gray (5B 4/1), dark gray (N 4), and gray (5Y 5/1) are interspersed in a greenish gray (5G 5/1 or 5GY 5/1) to dark greenish gray (5G 4/1) matrix and correlate with the glauconite-rich intervals in Cores 121-755A-13R to 121-755A-17R. The glauconite grains are large and granular, up to coarse sand size. In contrast, the tuff intervals with low glauconite concentrations are predominantly black (5Y 2.5/2), dark olive gray (5Y 3/2), and dark gray (5G 4/2) and increase in abundance toward the base of the subunit. Small fractures and vugs throughout this subunit are filled with secondary minerals, presumably pyrite and calcite. Subunit IIB is slightly to moderately bioturbated and mottled. Planar calcite laminae occur in Section 121-755A-13R-2. A 2–3-cm-thick gypsum-filled crack occurs in Section 121-755A-13R-1 (151.7 mbsf). Thin fractures, which are possibly clay partings, are more prevalent in the glauconite-poor intervals.

Subunit IIC consists of dark greenish gray (5BG 4/1) tuffs (60%–90% ash) with varying amounts of micrite. Glauconite-

Table 2. Lithologic units at Hole 755A.

Unit	Core interval	Depth (mbsf)	Age (Ma)	Lithology
I	1R–5R	0–65.5	Pleistocene–middle Miocene	Foraminifer nannofossil ooze, foraminifer nannofossil ooze with micrite, and nannofossil ooze with foraminifers
IIA	5R–12R	65.5–140.8	late Santonian–Coniacian/ Turonian	Tuff, tuff with micrite, and ashy limestone
IIB	13R–17R	140.8–189.0	Coniacian/ Turonian	Glauconitic tuff, tuff with glauconite, and tuff with glauconite and micrite
IIC	18R–19R	189.0–208.4	Coniacian/ Turonian	Tuff and tuff with micrite

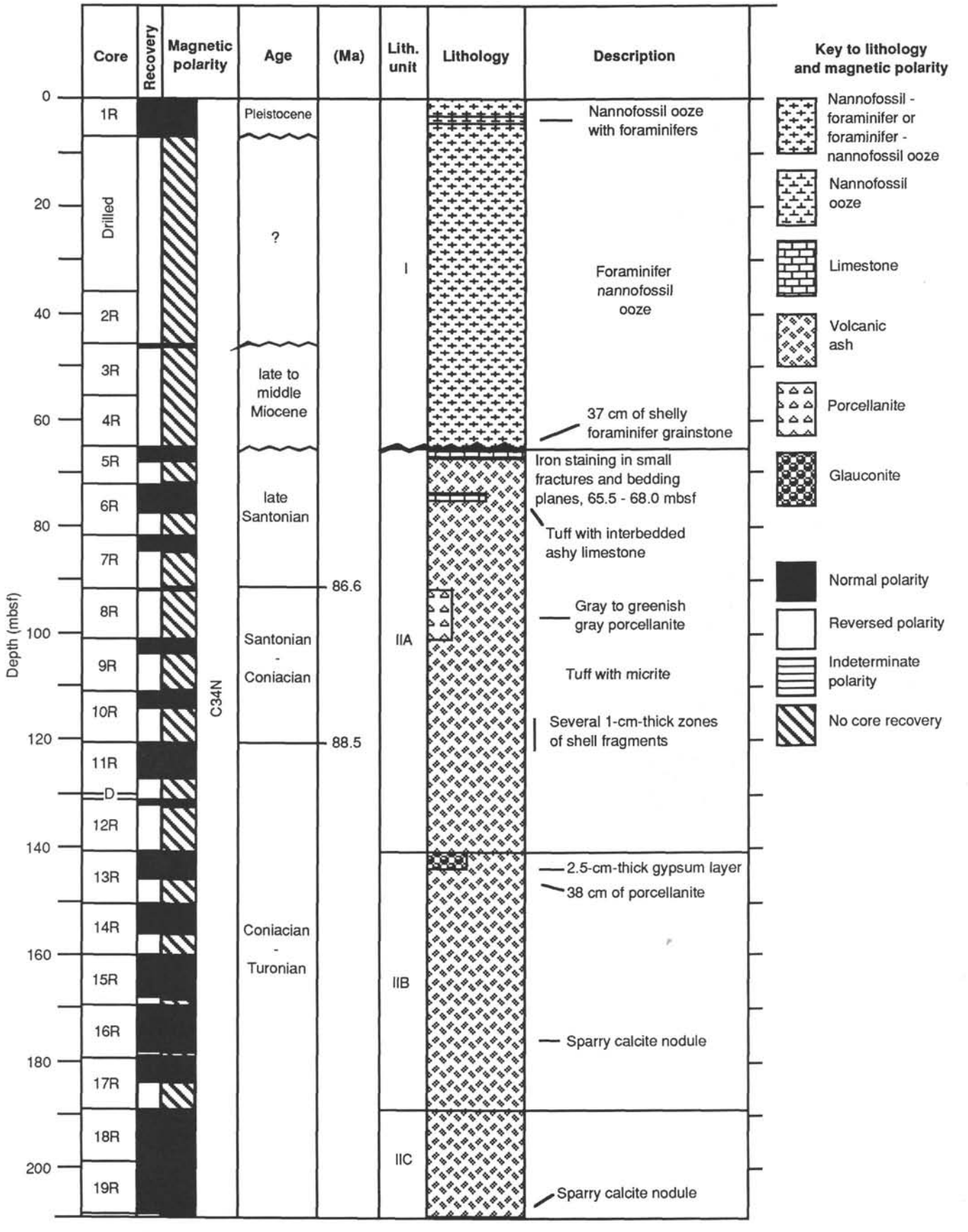

Figure 3. Site 755 summary diagram.

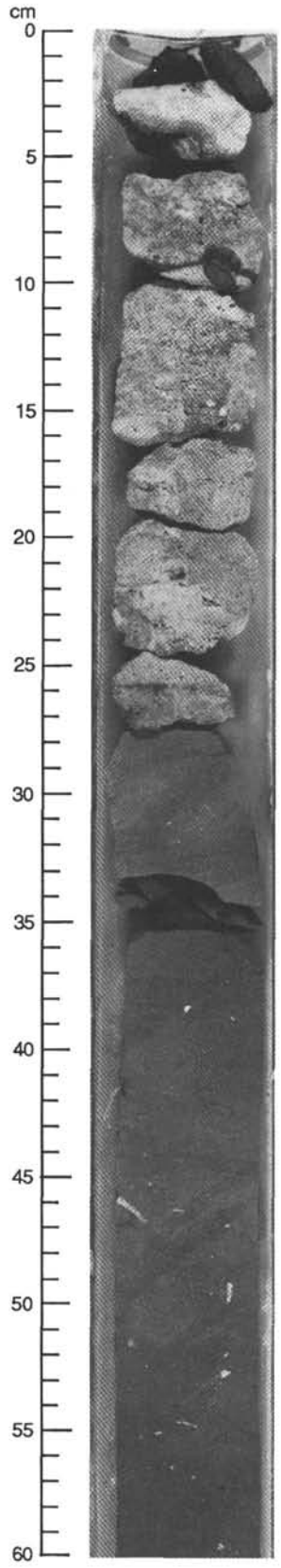

Figure 4. The sharp contact between the shelly foraminifer grainstone in lithologic Unit I and the underlying tuff with interbedded ashy limestone in lithologic Subunit IIA (Section 121-755A-5R-1, 0–60 cm).

rich intervals in Core 121-755A-18R have sharp basal contacts (at 47 cm in the core; Fig. 5) and fine upward. Light gray (N 7) to dark greenish gray (5BG 4/1) mottles becomes more pronounced in the subunit away from these coarse-sand intervals (Fig. 5). Some microfractures and vugs are filled with secondary and authigenic minerals, calcite, gypsum, and pyrite. Soft-sediment deformational structures occur in Core 121-755A-18R. Three essentially pure nodules of recrystallized gray (N 7) sparry limestone occur in Sections 121-755A-16R-5, 121-755A-19R-6, and 121-755A-19R-7 (Figs. 6 and 7).

Grain Size

Grain-size data were collected for the bulk sediments of Unit I in Core 121-755A-1R (Table 3). A description of the analytical procedure and equipment is in the "Explanatory Notes" chapter (this volume). The results of the grain-size data correlate well with the lithology. A minimum in the bulk-sediment grain size correlates to the nannofossil ooze with foraminifers in Section 121-755A-1R-3. In contrast, the maximum values for the bulk-sediment grain size are coincident with the foraminifer nannofossil ooze in Sections 121-755A-1R-1 and 121-755A-1R-4.

BIOSTRATIGRAPHY

The main objective of drilling at Site 755 was to penetrate as deeply as possible the lowermost part of the dipping and truncated sediments at Broken Ridge and recover a representative Cretaceous section of the basal dipping series. Time ran out and the drill string was pulled out before we reached the prominent acoustic basement reflector, dubbed the "Jersey Turnpike." However, in extrapolating sedimentation rates of 3 cm/1000 yr beyond 208 mbsf (Fig. 8 and Table 4), we expect the rocks below the "Jersey Turnpike" to be of Cenomanian age, if there is no major hiatus present.

Calcareous Nannofossils

Drilling at Site 755 recovered Pleistocene to middle Miocene (CN13–5) and upper Santonian(?) to Turonian sediments. The middle Miocene sediments unconformably overlie the upper Santonian deposits (Fig. 9). The Cretaceous nannofossils indicate an austral assemblage.

Neogene

The 65.2 m of foraminifer nannofossil ooze sampled in two spot cores at Site 755 contains a rich assemblage of Neogene calcareous nannofossils. The preservation is usually good. Core 121-755A-1R (0–7.1 mbsf) contains Pleistocene (Zone CN13) calcareous nannofossils, with species such as *Crenalithus doronicoides, Rhabdosphaera clavigera, Calcidiscus macintyrei, Pseudoemiliania lacunosa*, and *Helicosphaera sellii*. Sediments were not recovered between 7.1 and 45.8 mbsf. Samples 121-755A-3R-CC and 121-755A-4R-CC (55.5–65.2 mbsf) contain nannofossils of middle Miocene age (CN5/6), based on the presence of *Discoaster exilis, C. macintyrei*, and *Cyclicargolithus floridanus*.

Cretaceous

The greenish gray limestone/volcaniclastic unit below the foraminifer nannofossil ooze contains Late Cretaceous age nannofossils of late Santonian through Turonian age. The poor preservation and the scarcity of nannofossils in almost all sections prohibit a detailed biostratigraphic zonation.

Examinations of core-catcher "toothpick" samples show that some species, such as *Watznaueria barnesae, Tranolithus phacelosus, Zygodiscus compactus, Gartnerago obliquum*, and *Ahmuellerella octoradiata*, are consistently present in all sections. *Marthasterites furcatus* occurs in the upper part of the section.

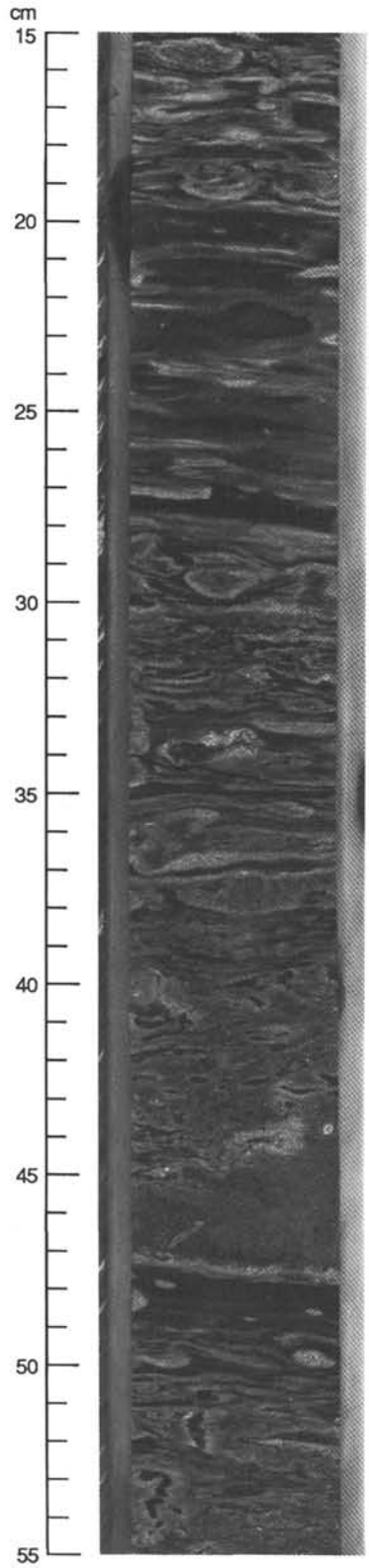

Figure 5. The sharp basal contact (47 cm) of the glauconite-rich sand layer, which becomes more burrowed as the grain size fines upward (Section 121-755A-18R-1, 15–55 cm).

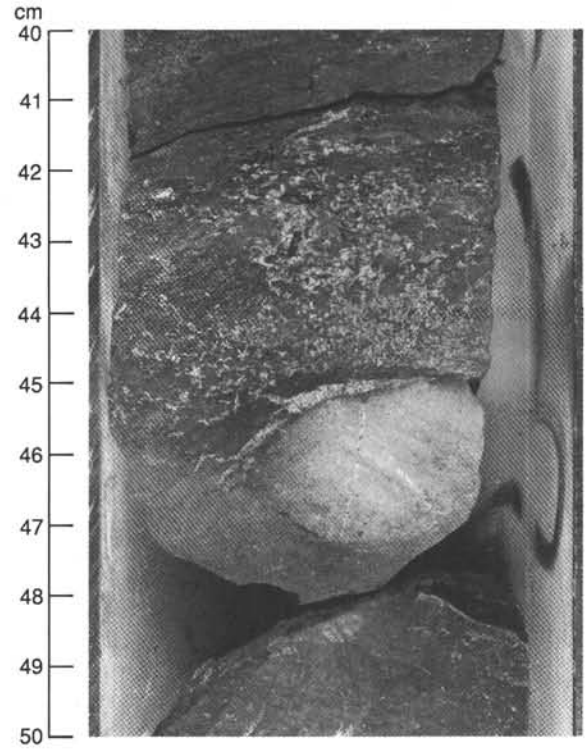

Figure 6. Recrystallized sparry calcite nodule at 45 to 47 cm in Section 121-755A-16R-5.

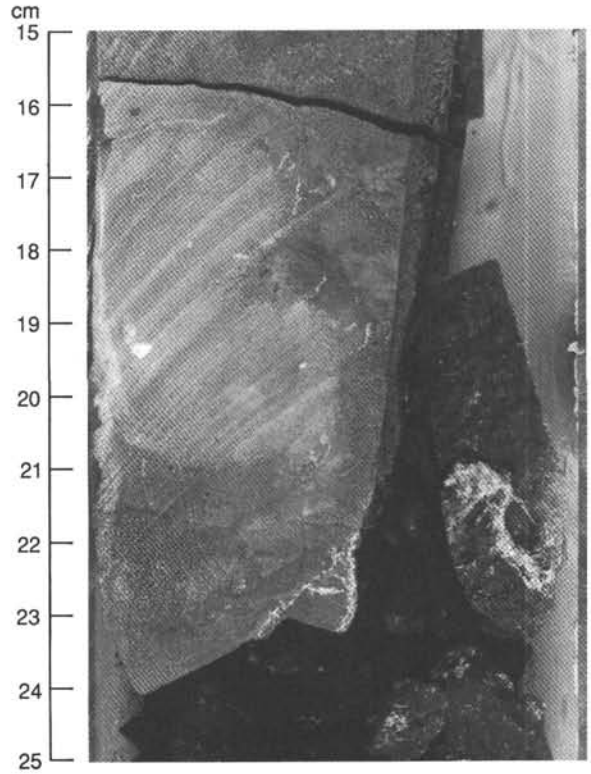

Figure 7. Recrystallized sparry calcite nodule at 16 to 20.5 cm in Section 121-755A-19R-7.

Table 3. Mean grain-size data, Hole 755A.

Core, section, interval (cm)	Depth (mbsf)	Mean grain size (μm)
1R-1, 60	0.60	79.7
1R-3, 120	4.20	38.9
1R-4, 40	4.90	88.4

The interval of Section 121-755A-5R-1 through Core 121-755A-7R (65.6–91.5 mbsf) is assigned to Zone CC15–16 (Santonian) of Sissingh (1977), based on the presence of *Micula decussata, Reinhardites anthophorus, Kamptnerius magnificus*, and *Aspidolithus parcus expansus*. Samples 121-755A-8R-CC to 121-755A-10R-CC (91.5–120.5 mbsf) are of CC14 (Santonian/Coniacian) age, as indicated by the presence of *M. decussata, K. magnificus*, and *A. parcus expansus* and the absence of *R. anthophorus*. The Coniacian and Santonian nannofossil assemblages cannot be subdivided into zones.

The first occurrence of *K. magnificus*, in Sample 121-755A-13R-CC, indicates a middle Turonian to Coniacian age (Thierstein, 1974, 1976). The determination of the Turonian/Coniacian boundary in Hole 755A is difficult, because the species that marks the boundary, *M. furcatus*, occurs only sporadically in the upper part of the section (65–72.1 mbsf).

Table 4. Datums used for calculating sedimentation rates at Site 755.

Datum	Age (Ma)	Depth (mbsf)
CN13	1.7–1.9	0–7.1
CN6	10–10.8	45.8–65.4
CN5	10.8–14.4	55.8–65.6
Unconformity	14.4–85	65.6
CC15	85–86.5	65.44–91.5
CC12	88.5–89	120.5–140.8
Globotruncana sigali/Globotruncana primitiva Zones	88–89.5	110.9–169.7

Sample 121-755A-18R-CC is barren of nannofossils. A toothpick sample of a short limestone interval from 123 to 124 cm in Section 121-755A-18R-2 contains an assemblage that is Coniacian-Turonian in age. Owing to the scarcity and poor preservation of the calcareous nannofossils, the zonation of the section

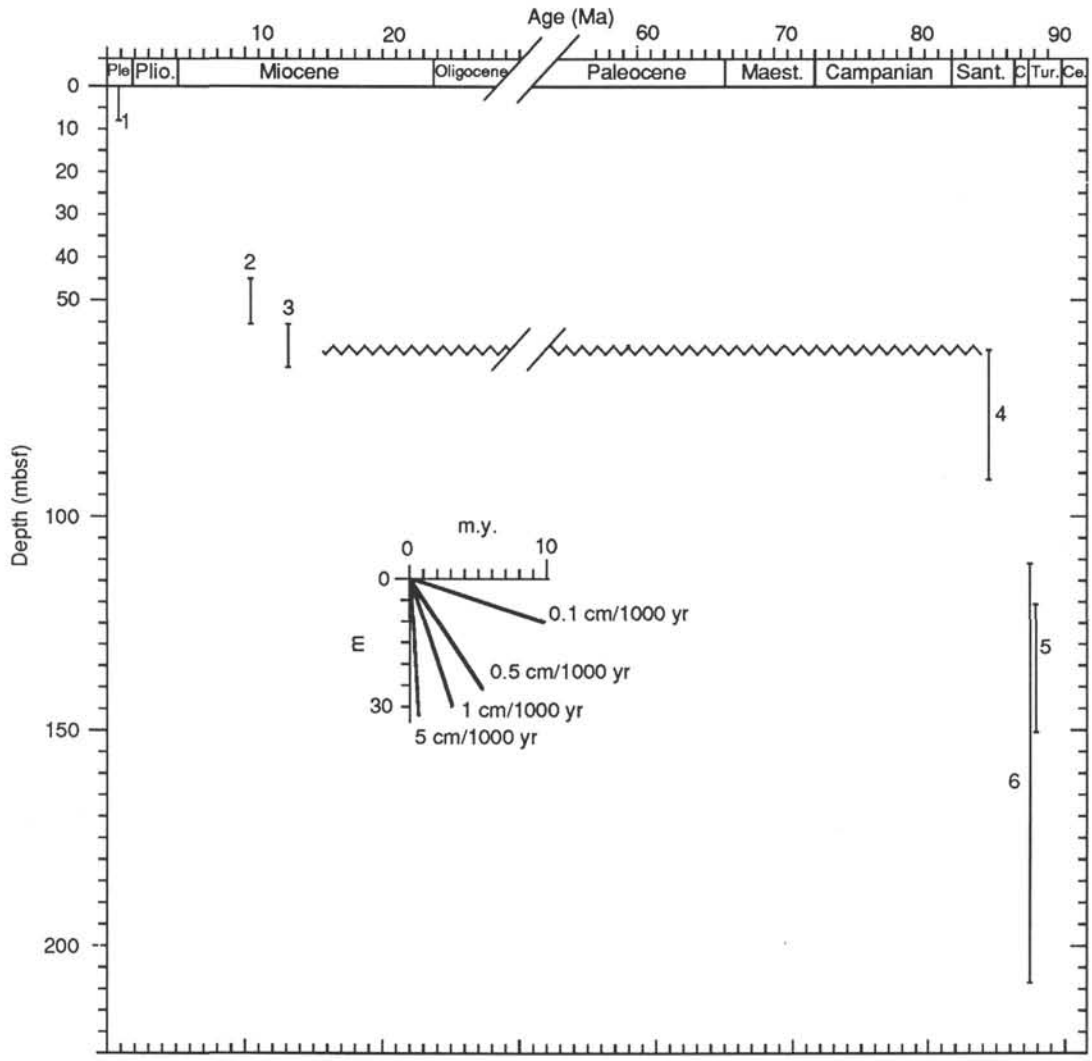

Figure 8. Age vs. depth plot for Site 755. Tie-points are based on the datums given in Table 4.

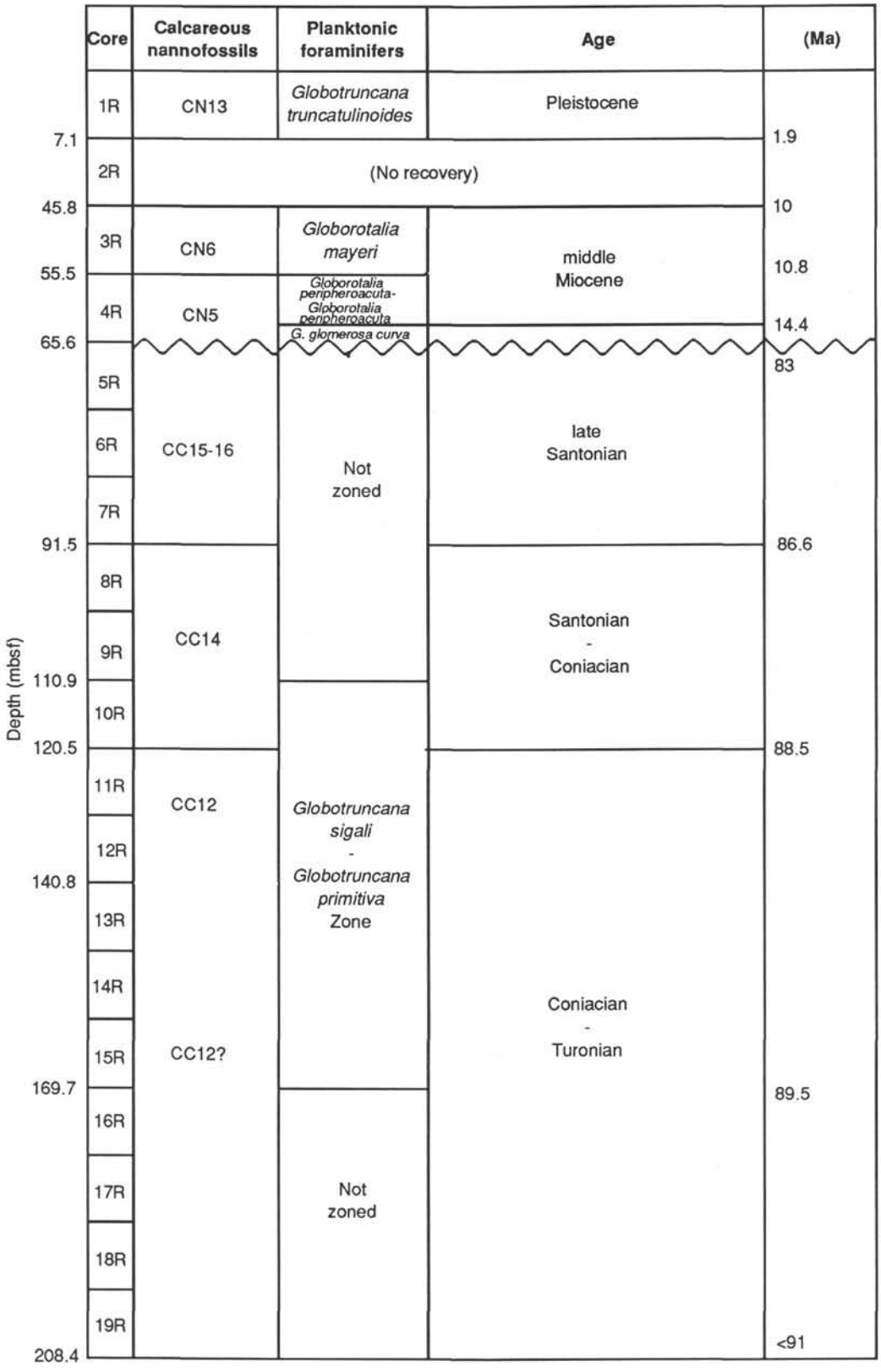

Figure 9. Calcareous nannofossil and planktonic foraminifer zones in Hole 755A.

is tentative. The presence of *G. obliquum* and *K. magnificus* is characteristic for austral, high-latitude assemblages (Thierstein, 1976). The absence of *Lucianorhabdus cayeuxii* and *Lucianorhabdus maleformis* may be due to ecological factors, because these two species are rare in open-ocean sediments. *M. furcatus* occurs sporadically and is usually rare in high-latitude sediments (Perch-Nielsen, 1985).

Planktonic Foraminifers

Neogene

The Neogene cap was sampled in two spot cores; Sample 121-755A-1R-CC yielded a Pleistocene age and Sample 121-755A-3R-CC a middle Miocene age. As at Sites 752, 753, and 754, the cap consists of winnowed foraminiferal nannofossil ooze. Sample 121-755A-3R-CC contains a well-preserved benthic fauna, with preserved delicate aragonite "mother-of-pearl" gastropod shells and even pteropod shells. Other fossils include bryozoans, brachiopods, corals, pelecypods, coralline algae, and crustacean remains such as barnacles and crab leg joints. Presumably most of the shallow-water fossil material has been washed down into bathyal depths. The base of the Neogene was reached at 65.5 mbsf, between 24 and 36 cm in Section 121-755A-5R-1, where dark discolored Santonian volcanogenic outer shelf sediments are overlain by a porous white shelly foraminiferal grainstone that yields latest early Miocene age planktonic foraminifers, such as *Praeorbulina glomerosa*.

Cretaceous

The section was continuously cored from 65.4 to 208 mbsf, and sediments of Santonian to Turonian age were recovered. The sediments are dark and contain abundant glauconite, glass shards, pumice, and other diagenetically altered volcanic products. As the volcanogenic component increases downsection, the amount of micritic limestone and chalk decreases and with it the abundance and preservation of the microfossils. Most of the lower part of this section is barren of planktonic foraminifers.

Planktonic foraminiferal determinations required making thin sections or thin slabs from limestone core-catcher material throughout the Cretaceous interval. The slabs were stained with methylene blue and then examined under a binocular microscope. Within the limestones the planktonic foraminifers seem well preserved, but when prepared as a washed residue, preservation ranked as poor. In the rocks with many volcanic shards, microfossils are commonly crushed.

Sample 121-755A-6R-CC yielded a Santonian planktonic foraminiferal fauna. Representatives of the *Globotruncana linneiana* and *Globotruncana lapparenti* group are common. Single-keeled forms of the *Globotruncana elevata–Globotruncana stuartiformis* group were not observed. The *Rugoglobigerina rugosa* group, common in the Campanian-Maestrichtian sediments of Hole 752B, was not found. Examination of slabs revealed essentially the same fauna down to Core 121-755A-10R. Sample 121-755A-13R-CC yielded representatives of the *Globotruncana coronata* group and the *Globotruncana primitiva* group, of late Turonian to early Coniacian age (Caron, 1985), the oldest well-preserved (in slabs) planktonic foraminiferal fauna of Hole 755A. Farther downsection, the core-catcher samples were almost barren of planktonic foraminifers, except for a few double-keeled *Globotruncana* sp. in Sample 121-755A-15R-CC.

In the few washed residues (e.g., Sample 121-755A-6R-CC) planktonic/benthic foraminiferal ratios are about 2 (except in Sample 121-755A-6R-CC, where the ratio is about 1). Ratios of about 2 are also found in the Maestrichtian to Danian of Samples 121-752A-32X-CC and 121-752B-12R-CC. The similar ratios between the sites suggests that Broken Ridge remained a platform at outer shelf–upper slope depths (200–500 m) throughout the Late Cretaceous and early Paleocene. The benthic foraminifers, however, suggest somewhat deeper, upper to middle bathyal depths.

Benthic Foraminifers

All >125-μm fractions of core-catcher samples from Site 755 were examined for benthic foraminifers. In Samples 121-755A-1R-CC and 121-755A-3R-CC Neogene benthic foraminifers are well preserved, in contrast to the Late Cretaceous age benthic foraminifers in Samples 121-755A-5R-CC through 121-755A-19R-CC.

Pleistocene

In Sample 121-755A-1R-CC, *Planulina wuellerstorfi* and *Cibicidoides* spp. are common. *Globocassidulina subglobosa, Karreriella bradyi, Fissurina* spp., and *Paracassidulina* spp. were found frequently, along with a few specimens of *Sphaeroidina bulloides, Ehrenbergina trigona, Oridorsalis umbonatus*, and *Ammosphaeroidina sphaeroidiformis*. This fauna is characteristic of middle to lower bathyal depths and is compatible with the present depth of Site 755 (1058 m).

Miocene

The Miocene fauna in Sample 121-755A-3R-CC is characterized by the abundance of *Globocassidulina* spp. "*Karreriella*" spp., *Gyroidina soldani, O. umbonatus, Laticarinina pauperata, Uvigerina* sp., *Pullenia bulloides*, and *Ehrenbergina hystrix* are also common. This faunal composition is comparable to the middle Miocene faunas of Samples 121-754A-8H-CC to 121-754A-13H-CC and is typical of middle to lower bathyal depths.

Surprisingly, poorly preserved shallow-water mollusks, bryozoans, and coral fragments were found in the same sample (121-755A-3R-CC). Such inclusions clearly contradict the aforementioned benthic faunal character and suggest some downslope transport.

Cretaceous

Cretaceous faunas of Santonian to Turonian age are of low diversity and show low abundance of benthic foraminifers. No foraminifers were found in Samples 121-755A-12R-CC, 121-755A-14R-CC, and 121-755A-18R-CC. The taxa found in the other samples are *Gavelinella, Allomorphina, Ellipsoidella, Dorothia, Astacolus, Gyroidinoides, Lenticulina*, and *Vulvulineria*. Thin-shaped *Gavelinella* sp. was found almost continuously.

Typical deep-water taxa were not found in the core-catcher samples of Site 755. Therefore, we assume that the assemblages indicate upper bathyal depths in the Santonian and Turonian.

Associated fossils include a few *Inoceramus* prisms, fish debris, and echinoid spines.

Diatoms

No diatoms were found in the core-catcher samples of Site 755. Rare and poorly preserved radiolarians and sponge spicules are present in Samples 121-755A-5R-CC, 121-755A-11R-CC, 121-755A-12R-CC, 121-755A-16R-CC, and 121-755A-17R-CC. Radiolarians were found to be somewhat more abundant in Sample 121-755A-11R-CC, a sample with relatively organic-rich (<1.0%) laminae (see "Organic Geochemistry" section, this chapter).

PALEOMAGNETICS

Paleomagnetic analysis of the sedimentary sequence at Site 755 consisted of whole-core susceptibility and natural remanent magnetization (NRM) measurements (initial NRM and after 9-mT demagnetization) of archive core halves. An additional 17 samples were partially stepwise demagnetized in an alternating field (AF) of up to 20 mT in order to confirm the polarity interpretation reached from analysis of the archive core-half results.

Susceptibility

The susceptibility record (Fig. 10) for the Upper Cretaceous sequence shows high susceptibility values in the upper part of the sequence (lithologic Subunit IIA and the top of Subunit IIB; Cores 121-755A-5R to 121-755A-13R; 65.2–156.4 mbsf). The base level susceptibility is between 20 × 10^{-6} and 100 × 10^{-6} cgs units, with spikes up to 200 × 10^{-6} to 800 × 10^{-6} cgs units. Very high values were found in the lower part of the hole (most of Subunit IIB and all of Subunit IIC; Cores 121-755A-14R to 121-755A-19R; 150.4–208.4 mbsf). Base level susceptibility was as high as 500 × 10^{-6} cgs units, with spikes up to 1700 × 10^{-6} cgs units. These high susceptibilities largely reflect the high to very high ash content throughout the sequence (see "Lithostratigraphy and Sedimentology" section, this chapter). Core 121-755A-12R (131.1–140.8 mbsf) is a notable exception, with a substantially lower susceptibility base level (< 5 × 10^{-6} cgs units).

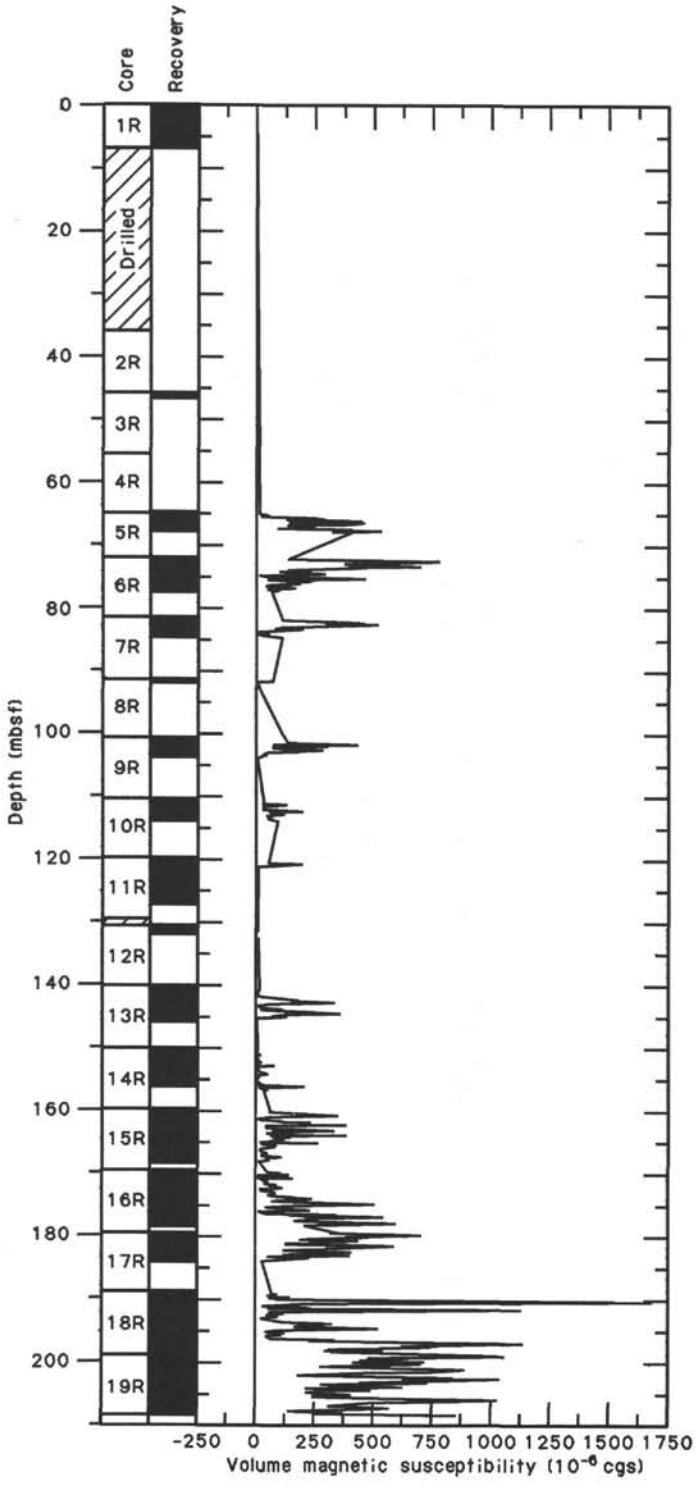

Figure 10. Whole-core susceptibility data for Hole 755A.

The susceptibility record (Fig. 10) shows a pattern of gradual increases/decreases in both the base level and in the peak level of susceptibility spikes. A large-scale gradual increase in susceptibility with younger age occurs through Cores 121-755A-19R to 121-755A-18R (208.4–189.0 mbsf) and is followed by a decrease through Cores 121-755A-17R to 121-755A-14R (189.0–150.4 mbsf). Similar variations, but on a smaller scale, are visible through Cores 121-755A-17R to 121-755A-16R (189.0–169.7 mbsf), 121-755A-15R to 121-755A-14R (169.7–150.4 mbsf), 121-755A-13R (140.8–150.9 mbsf), 121-755A-7R (81.8–91.5 mbsf), and 121-755A-6R (72.1–81.8 mbsf). The lithologic description of Hole 755A suggests that these susceptibility variations primarily reflect variations in ash content, rather than mineralogical variations. If so, the susceptibility record may reflect a buildup of eruptive volcanic activity from the base of the recovered sequence (Core 121-755A-19R) to a paroxysmal eruptive phase recorded at 190 mbsf. A gradual decrease in activity is recorded up to 150 mbsf, which was followed by more sporadic eruptive phases of either lesser magnitude or, possibly, occurring at a greater distance.

Remanence

The NRM intensity record of archive core halves essentially mirrors the susceptibility pattern, particularly after AF demagnetization at 9 mT (Fig. 11), which is relatively free of disturbing magnetic overprints. The upper part of the Upper Cretaceous sequence (lithologic Subunit IIA and very top of Subunit IIB; Cores 121-755A-5R to 121-755A-13R; 65.2–150.4 mbsf) has NRM intensities ranging from 1 to 100 mA/m, whereas NRM intensities in the lower part of the sequence (most of Subunit IIB and all of Subunit IIC; Cores 121-755A-14R to 121-755A-19R; 150.4–208.4 mbsf) vary between 10 to 500 mA/m. Peaks in NRM intensity at 190.3, 145–144, and 104–101 mbsf are directly correlatable with spikes in the susceptibility record (compare Figs. 10 and 11). The high susceptibility and NRM intensities and moderate median demagnetizing fields suggest that magnetite or titanomagnetite is the dominant magnetization carrier.

Magnetostratigraphy

The 9-mT remanence record (Fig. 11) and discrete sample demagnetization studies (Fig. 12) clearly demonstrate the exclusively normal polarity record of the recovered sequence, which falls entirely within the Cretaceous Normal Polarity Interval (Chron C34N; Berggren et al., 1985; Bolli et al., 1985). A single observation of reversed polarity at the base of Section 121-755A-12R-1 (131.1–140.8 mbsf) (Fig. 11) is probably the result of misorientation of the core pieces during recovery of this badly fragmented core.

INORGANIC GEOCHEMISTRY

The objectives of the inorganic geochemistry studies for Leg 121 are given in the "Inorganic Geochemistry" section, "Site 752" chapter. A summary of the overall results for the Broken Ridge section of Leg 121 is given in the "Broken Ridge Summary" chapter.

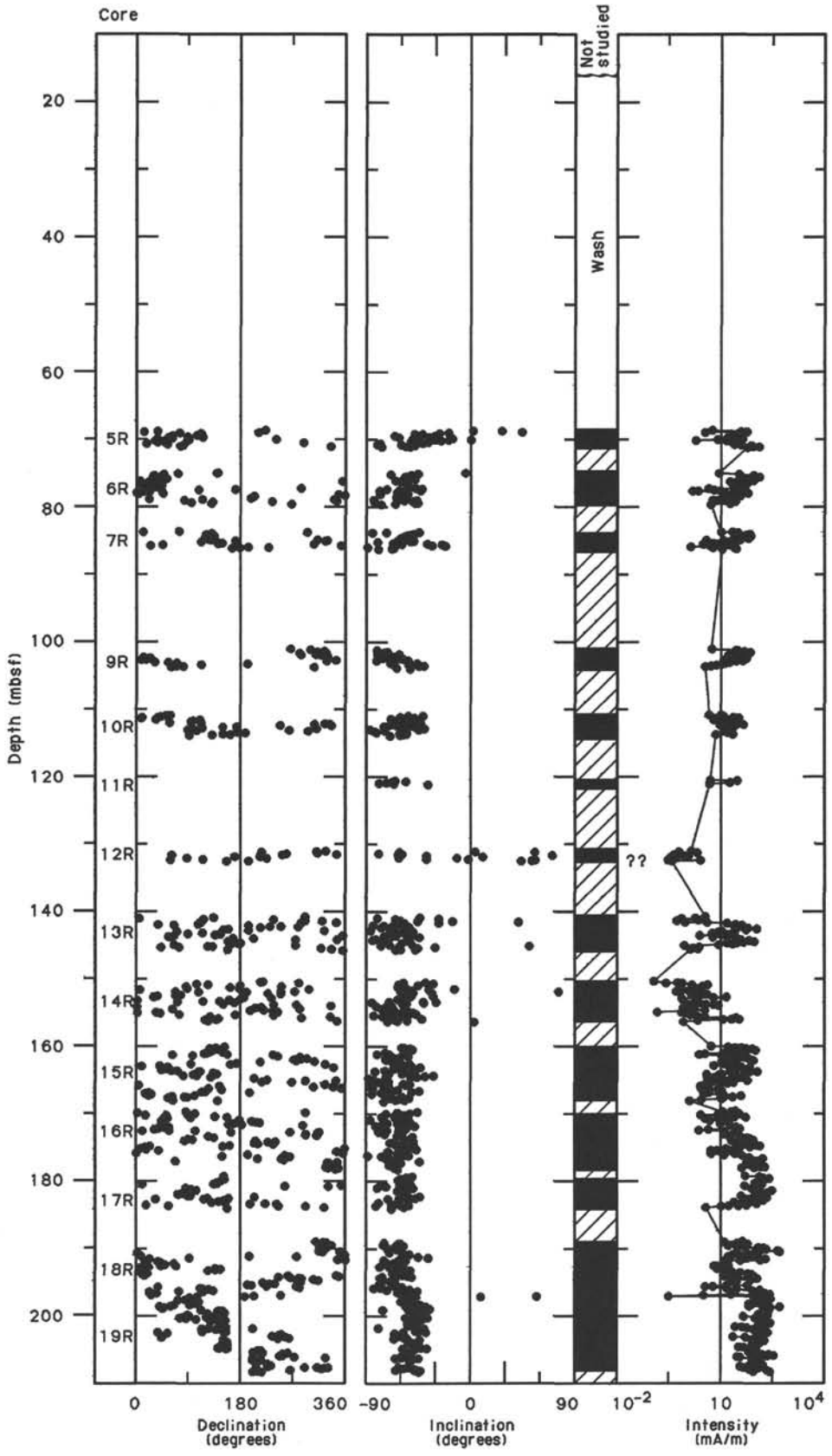

Figure 11. Remanence intensities of archive core halves from Hole 755A after AF demagnetization at 9 mT. Black represents normal polarity; diagonal lines indicate no recovery.

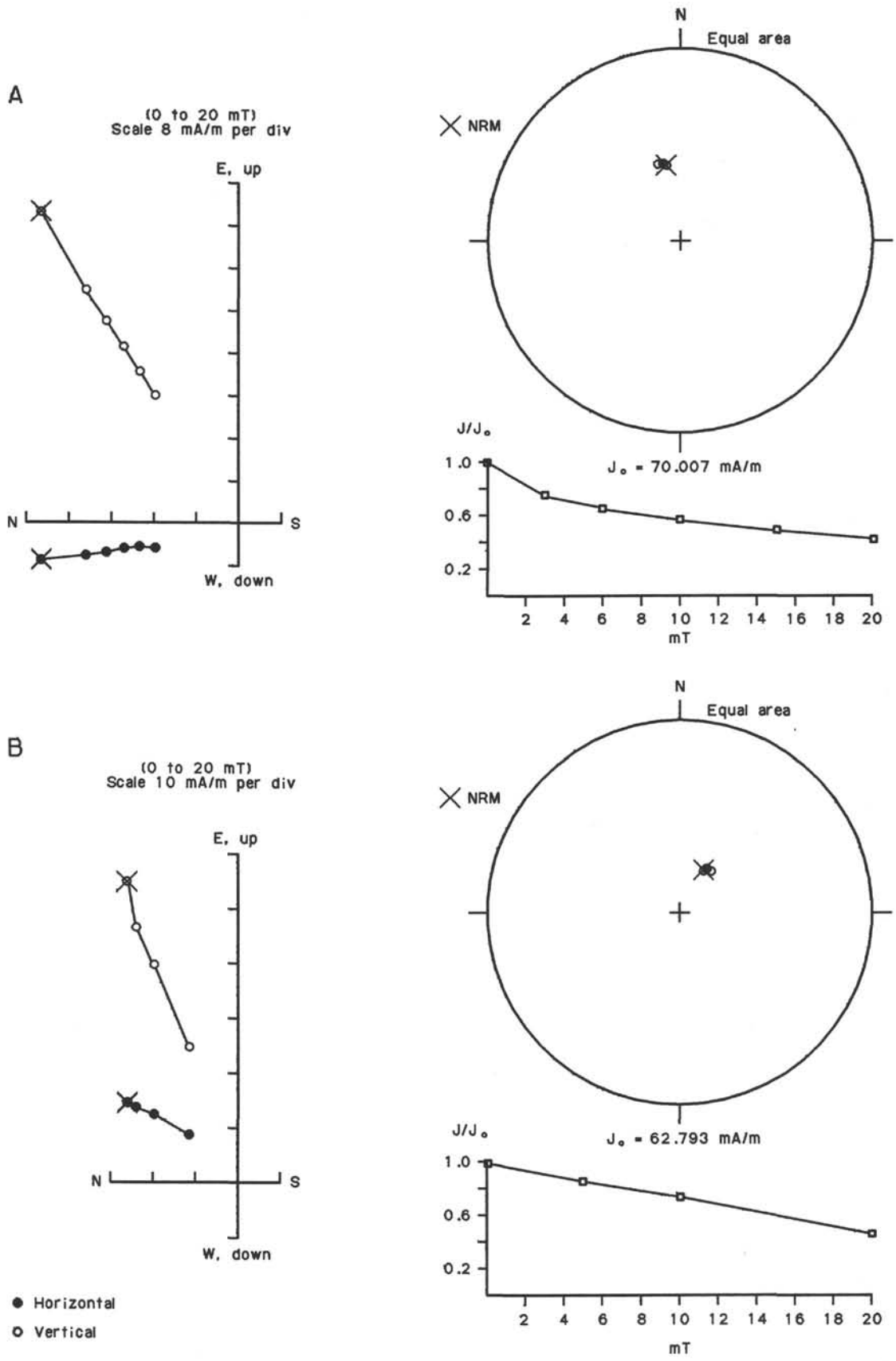

Figure 12. Zijderveld, equal area, and intensity decay plots indicating normal polarity (Chron C34N). **A.** Sample 121-755A-11R-1, 12–14 cm. **B.** Sample 121-755A-15R-3, 31–33 cm.

Results

The chemical compositions of the pore waters are similar to those of Site 754, although only four intervals were sampled at Site 755. As at Site 754, sampling ceased as soon as lithified rocks were encountered below the angular unconformity. A single sample was obtained below the unconformity at each site. In both instances relatively small amounts of pore waters were squeezed from the sediments (see Table 5). Calcium, magnesium, and sulfate ion concentrations and alkalinities were only slightly changed from seawater values above the unconformity at both sites. Although chloride concentrations changed at both sites, the changes were barely significant relative to measurement error. The suggested squeezing effects described for Site 754 ("Inorganic Geochemistry" section) did not show up at Site 755.

Discussion

The lack of an "ash" signal at Sites 754 and 755 similar to that found at Sites 752 and 753 divides the four sites drilled on Broken Ridge into two groups. Where significant quantities of ash were found in unlithified sediments, large increases in calcium and magnesium in the pore waters were observed. Where altered ashes were found (only in the highly lithified sediments below the unconformity), very small changes in calcium and magnesium were observed. In summary, the overall chemical patterns in the pore waters of Broken Ridge appear to be controlled primarily by stratigraphic and lithologic factors.

ORGANIC GEOCHEMISTRY

Samples from Site 755 were studied for their carbonate carbon and organic carbon contents and for concentrations of hydrocarbon gases. The methods used are described in the "Explanatory Notes" chapter.

Hydrocarbon Gases

Methane concentrations do not exceed 10 ppm in any of the headspace gas analyses. Ethane and propane were not detected.

Organic Carbon Content and Character

In the Cretaceous section cored between 65 and 208 mbsf, organic carbon percentages do not exceed 1% and are generally in the range of 0.1%–0.3% (Table 6 and Fig. 13). Thus, organic matter contents at Site 755 are only slightly higher than those in the Tertiary and Maestrichtian sections drilled at Sites 752, 753, and 754. This reveals that "anoxic events" that would allow the preservation of a large proportion of the sedimentary biogenic organic matter did not occur during the deposition of the sediments cored at Broken Ridge.

Sample 121-755A-14R-2, 137–138 cm, with an "extraordinarily" high organic carbon content of 1%, is characterized by a mineralogic composition different from most of the sediments recovered at the Broken Ridge sites. Its major constituents are quartz and illite, with minor amounts of calcite and kaolinite.

The organic matter in the Cretaceous sediments at Site 755 is generally hydrogen lean (Table 7), which is similar to the younger sediments at Broken Ridge. Organic matter in the Neogene section is completely inert.

Carbonate Carbon Content

The carbonate content at Site 755 is significantly lower than in the younger sediments drilled at the other Broken Ridge sites (Table 6 and Fig. 13). On average, carbonate content decreases from about 30% in the Santonian to less than 10% in the Coniacian-Turonian. A summary of carbonate content for all Broken Ridge sites is presented in the "Broken Ridge Summary" chapter.

PHYSICAL PROPERTIES

The sediments cored at Site 755 consist of a Neogene (Pleistocene to uppermost lower Miocene) winnowed ooze sequence separated from an Upper Cretaceous tuff with micrite and glauconite by an angular unconformity at about 65 mbsf (Section 121-755A-5R-1). The section was rotary cored, with an average recovery of 45%. The samples tested (except one thermal-conductivity sample at 120.57 mbsf) are judged to be of good quality for physical-properties measurements.

Methods

Sediments from this site were measured for index properties, compressional-wave velocity, vane shear strength, formation factor, and thermal conductivity. The description of these methods is found in the "Explanatory Notes" chapter. Measurements of vane shear strength and formation factor were made only in the soft sediment cover (two measurements).

Results

Index Properties

Water content (expressed as water weight relative to wet sample weight), porosity, bulk density, dry-bulk density, and grain (or matrix) density of the Site 755 sediments are listed in Table 8 and plotted relative to depth in Figure 14. There is a large gap in the physical-properties data between 5 and 66 mbsf because of a washed interval and poor recovery. The sediment bulk density in the topmost layer (foraminifer nannofossil ooze) is approximately 1.65 g/cm^3. Below the unsampled zone, densities range from 2.0 to 2.47 g/cm^3 (tuff and ashy limestone). There is a slight increase at 92 mbsf (2.47 g/cm^3 maximum value), which is followed by a slight decrease (2.00 g/cm^3 minimum value) in the interval from 104 to 114 mbsf. Below this depth, densities average 2.3 g/cm^3 to the bottom of the hole. The changes in bulk density and other index properties are linked to lithologic changes, related mainly to the ash, glauconite, and micrite content of the sediments. High bulk-density values were obtained from two recrystallized calcite nodules in sediment near the base of the hole.

Grain density decreases gradually throughout the hole, from a value of approximately 2.7 g/cm^3 in the nannofossil ooze to 2.5 g/cm^3 in a Turonian tuff with micrite. There is a slightly increasing trend in grain density from approximately 125 to 140 mbsf, from where the values gradually decrease to 180 mbsf. The decrease can be correlated with lithologic Subunit IIB (141–

Table 5. Site 755 interstitial-water geochemistry data.

Core, section, interval (cm)	Depth (mbsf)	Volume (mL)	pH	Alkalinity (mmol/L)	Salinity (g/kg)	Magnesium (mmol/L)	Calcium (mmol/L)	Chloride (mmol/L)	Sulfate (mmol/L)	Mg^{2+}/Ca^{2+}
1R-1, 0–1	0.00	10			35.0	52.00	10.60	557.00	30.00	4.91
1R-4, 145–150	5.95	27	7.70	2.710	35.0	51.30	11.50	559.00	29.10	4.46
3R-1, 0–1	45.80	25	7.60	2.130	37.5	52.30	10.80	570.00	29.70	4.84
5R-1, 140–150	66.60	5			36.5	44.60	12.20	571.00	30.30	3.66

Table 6. Percentages of total carbon, inorganic carbon, organic carbon, and calcium carbonate in samples from Hole 755A.

Core, section, interval (cm)	Depth (mbsf)	Total carbon (%)	Inorganic carbon (%)	Organic carbon (%)	Calcium carbonate (%)
1R-3, 120–122	4.20	11.56	11.53	0.03	96.0
1R-4, 40–42	4.90	11.47	11.48	0.00	95.6
5R-1, 89–91	66.09	7.52	7.42	0.10	61.8
5R-2, 89–91	67.59		1.18		9.8
5R-CC, 0–1	67.99	0.53	0.47	0.06	3.9
6R-1, 56–58	72.66		2.43		20.2
6R-2, 89–90	74.49		7.63		63.6
6R-4, 38–40	76.98	4.22	4.06	0.16	33.8
7R-2, 72–75	84.02		1.57		13.1
7R-2, 89–90	84.19	1.86	1.69	0.17	14.1
8R-1, 30–32	91.80	0.81	0.69	0.12	5.8
9R-1, 128–131	102.48		1.99		16.6
9R-2, 80–82	103.50	2.50	2.43	0.07	20.2
10R-1, 27–29	111.17	0.60	0.49	0.11	4.1
10R-2, 89–91	113.29	4.47	4.42	0.05	36.8
10R-2, 121–123	113.61	2.48	2.37	0.11	19.7
10R-CC, 0–1	114.07	1.56	1.49	0.07	12.4
11R-1, 32–34	120.82	1.92	1.70	0.22	14.2
11R-1, 38–40	120.88	1.29	1.22	0.07	10.2
12R-1, 1–4	131.11		2.25		18.7
12R-1, 82–84	131.92	2.00	1.71	0.29	14.2
13R-2, 56–58	142.80	0.55	0.38	0.17	3.2
13R-2, 107–108	143.31	1.57	1.33	0.24	11.1
13R-3, 75–78	144.35		2.49		20.7
13R-3, 79–81	144.39	0.96	0.72	0.24	6.0
14R-2, 62–65	152.52		2.26		18.8
14R-2, 68–70	152.58	3.36	3.12	0.24	26.0
14R-2, 137–138	153.27	1.94	0.98	0.96	8.2
14R-3, 64–66	153.97	1.05	0.94	0.11	7.8
14R-CC, 0–1	156.33	1.56	1.44	0.12	12.0
14R-CC, 7–9	156.40	0.76	0.62	0.14	5.2
15R-1, 35–37	160.35	1.33	1.13	0.20	9.4
15R-3, 39–41	163.34	4.52	4.35	0.17	36.2
15R-5, 18–20	165.96	0.53	0.34	0.19	2.8
16R-2, 98–99	172.12	0.77	0.48	0.29	4.0
16R-4, 115–116	175.17	0.66	0.45	0.21	3.8
16R-6, 79–80	177.70	0.49	0.38	0.11	3.2
17R-2, 113–114	181.91	0.50	0.31	0.19	2.6
18R-2, 119–120	190.79	2.76	2.52	0.24	21.0
18R-4, 139–140	193.99	0.79	0.53	0.26	4.4
18R-6, 104–105	196.64	0.61	0.38	0.23	3.2
18R-6, 123–125	196.83		0.21		1.8
19R-2, 122–123	201.42	0.24	0.04	0.20	0.3
19R-4, 86–87	204.06	0.53	0.39	0.14	3.3
19R-6, 102–103	207.22	0.57	0.12	0.45	1.0
19R-6, 127–130	207.47		0.32		2.7

189 mbsf), which progressively changes from a glauconitic tuff to tuff with glauconite and micrite with depth. Glauconite possibly has a heavier grain density than glauconite with micrite, which would explain the decreasing trend in grain density. Subunit IIC (189–208 mbsf) consists of tuff with micrite. Water content, which is slightly above 40% in the oozes, decreases in the tuffs with micrite and glauconite to values of 10% to 20%. A small decrease was observed between 92 and 104 mbsf, where the lithology changes from a tuff with micrite into ashy limestone.

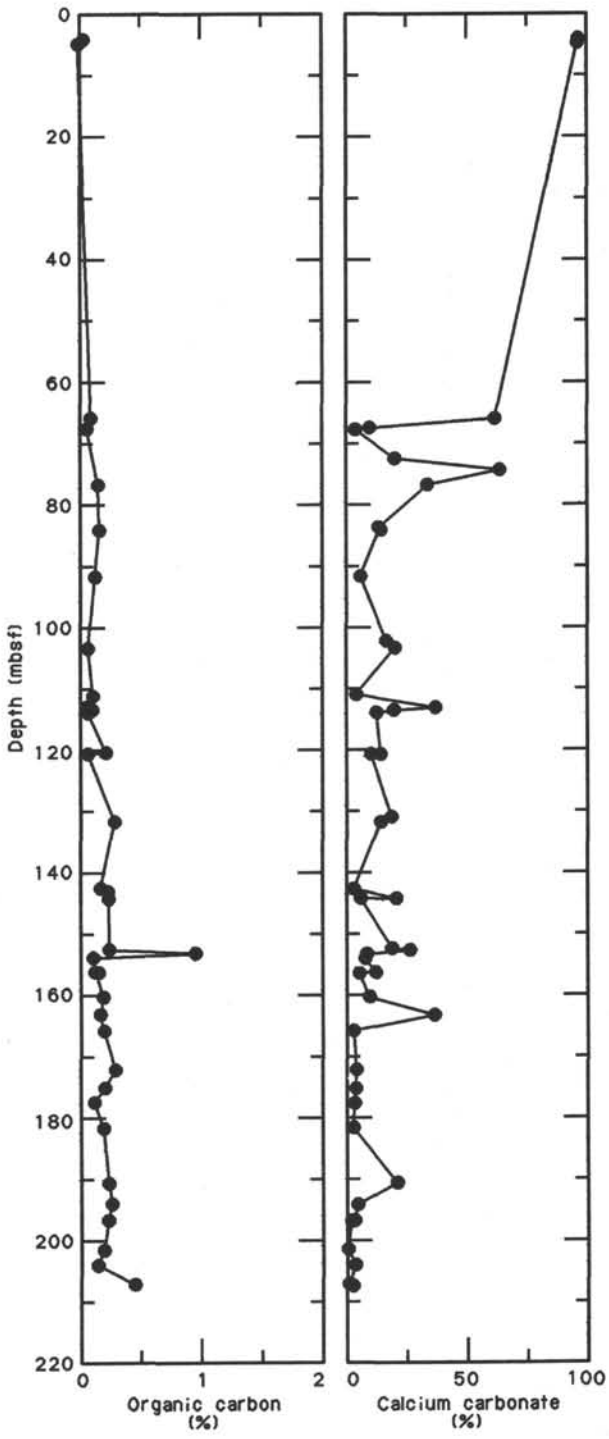

Figure 13. Organic carbon and calcium carbonate contents of samples from Site 755.

Table 7. Results of Rock-Eval pyrolysis of samples from Hole 755A.

Core, section, interval (cm)	Depth (mbsf)	Weight (mg)	T_{max} (°C)	S1 (mg HC/g rock)	S2 (mg HC/g rock)	S3 (mg CO_2/g rock)	Productivity index	S2/S3	Pyrolysized carbon (0.083 [S1 + S2])	Total organic carbon (wt%)	Hydrogen index (mg HC/g C_{org})
12R-1, 82–84	131.92	103.6	412	0.08	0.23	0.46	0.27	0.50	0.02	0.29	79
14R-2, 137–138	153.27	101.1	417	0.02	0.79	0.34	0.02	2.32	0.06	0.96	82
16R-2, 98–99	172.12	99.1	424	0.06	0.01	0.25	1.00	0.08	0.00	0.29	3
19R-6, 102–103	207.22	95.9	361	0.04	0.03	0.37	0.67	0.08	0.00	0.45	6

Table 8. Index properties of sediments from Hole 755A.

Core, section, interval (cm)	Depth (mbsf)	Water content (%)	Porosity (%)	Density		
				Wet bulk (g/cm^3)	Dry bulk (g/cm^3)	Grain (g/cm^3)
1R-3, 120	4.20	39.18	62.65	1.67	1.02	2.63
1R-4, 40	4.90	44.31	68.17	1.60	0.89	2.72
5R-1, 89	66.09	11.34	25.10	2.36	2.09	2.66
5R-2, 89	67.59	16.80	33.75	2.14	1.78	2.56
6R-2, 89	74.49	9.95	21.92	2.34	2.11	2.58
6R-4, 38	76.98	15.38	31.85	2.18	1.85	2.61
7R-2, 89	84.19	18.06	36.66	2.15	1.76	2.67
8R-1, 30	91.80	6.25	13.80	2.47	2.32	2.44
9R-2, 80	103.50	11.93	25.78	2.26	1.99	2.61
10R-1, 27	111.17	21.57	40.62	2.00	1.57	2.52
10R-2, 89	113.29	15.69	31.89	2.17	1.83	2.55
10R-2, 121	113.61	19.26	38.75	2.12	1.71	2.69
11R-1, 32	120.82	15.96	33.32	2.23	1.87	2.67
11R-1, 39	120.89	17.96	36.06	2.11	1.74	2.62
12R-1, 82	131.92	17.06	34.67	2.18	1.81	2.62
13R-2, 56	142.80	15.98	34.58	2.31	1.94	2.82
13R-3, 79	144.39	16.92	35.64	2.26	1.88	2.76
14R-2, 68	152.58	14.42	30.55	2.29	1.96	2.65
14R-3, 64	153.97	16.00	32.59	2.22	1.86	2.58
14R-5, 7	156.40	9.55	21.48	2.43	2.20	2.63
15R-1, 35	160.35	13.36	29.20	2.33	2.02	2.72
15R-3, 39	163.34	13.44	28.44	2.31	2.00	2.60
15R-5, 18	165.96	13.01	27.98	2.28	1.98	2.64
16R-2, 98	172.12	11.54	24.67	2.33	2.06	2.55
16R-4, 115	175.17	14.83	30.47	2.20	1.88	2.56
16R-6, 79	177.70	15.30	30.92	2.17	1.83	2.52
17R-2, 113	181.91	14.26	28.11	2.18	1.87	2.39
18R-2, 119	190.79	12.06	25.28	2.37	2.08	2.51
18R-4, 139	193.99	15.01	30.89	2.20	1.87	2.57
18R-6, 104	196.64	12.81	25.94	2.17	1.89	2.42
19R-2, 122	201.42	17.50	35.18	2.15	1.78	2.60
19R-4, 86	204.06	16.24	33.08	2.18	1.83	2.59
19R-6, 102	207.22	14.25	29.03	2.22	1.90	2.50

Note: The interval between 4.90 and 66.09 mbsf was not sampled.

The porosity in the Neogene oozes ranges from 60% to 70% and decreases in the Santonian tuffs to between 20% to 40% (Fig. 14). There is a small minimum at 92 mbsf, as observed in a water-content curve. Below that depth, porosity increases to local maximum of 35%, from which it gradually decreases toward the bottom of the hole to values of approximately 30%. This decrease can be explained by increased compaction and lithification. The dry-bulk-density curve is almost a mirror image of the porosity curve (Fig. 14). Dry-bulk density in the oozes (about 1 g/cm^3) increases to values of about 1.9 g/cm^3 in the tuffs.

Compressional-Wave Velocity

Velocity data collected with the *P*-wave logger and on a Hamilton Frame are displayed in Table 9 and Figure 14. Velocities collected in the ooze with the *P*-wave logger are around 1500 m/s. Velocities in the tuffs are around 2600 m/s, with several peaks reaching velocities over 4000 m/s. The first peak is in Santonian tuffs (3917 m/s at 114 mbsf) and coincides with rock described in the visual core description as much harder than the overlying limestone. The next, and highest, velocity peak is in the Coniacian tuff (4067 m/s at 121 mbsf). There are more velocity peaks at 133, 155, and 162 mbsf. The velocity increases (except for the first one) are not related to the general tuff lithology as they are at Site 752, where velocity decreases correlated with ash layers. Measurements of velocity anisotropy of limestones were performed at this site. We found (as at Sites 752 and 754) that the compressional-wave velocities are up to 10% slower in the vertical direction (see "Physical Properties" section, "Site 754" chapter, this volume). Velocities in excess of 4000 m/s were also measured in recrystallized calcite nodules recovered from below 170 mbsf.

The impedance log computed from GRAPE measurements (several values in the first 5 m of sediments), bulk-density values, and velocity data shows several impedance contrasts. The contrasts occur at the top of the Santonian ashy limestone layer (78 mbsf), at the boundary between two lithologic types (tuff with interbedded ashy limestone and tuff with micrite) at 82 mbsf (see "Lithostratigraphy and Sedimentology" section), in a tuff with glauconite layer (162 mbsf), and in Coniacian-Turonian tuff layers (171 and approximately 190 mbsf). These impedance contrasts are possible downhole sources of reflected seismic energy (see "Seismic Stratigraphy" section, this chapter). The impedance contrasts are almost entirely caused by increases in seismic velocity.

Vane Shear Strength and Formation Factor

Two measurements of undrained shear strength and formation factor were obtained in the first core of Hole 755A sediments. The values are consistent with values obtained at the other sites on Broken Ridge.

Thermal Conductivity

Thermal-conductivity data are shown in Table 10 and Figure 14. The first two samples taken in the Neogene ooze have thermal conductivities of 1.3 and 1.8 W/m°C. The next sample value is 1.4 W/m°C at 66 mbsf. From this value the thermal conductivity evenly increases up to 2.7 W/m°C at 132 mbsf. The sample value at 121 mbsf (dark greenish gray, faintly mottled and bioturbated tuff) is exceptionally low (1.12 W/m°C) and appears in the middle of an increasing trend. This low value is suspect. Thermal conductivity decreases from 132 mbsf to the bottom of hole, where it reaches 1.4 W/m°C. There is a small secondary peak at 182 mbsf. Maximum thermal-conductivity values correspond, approximately, to the change in lithology between Coniacian-Turonian limestone with ash and limestone with glauconite. The subtle increase at 180 mbsf marks a lithology change between limestone and ashy limestone and tuff. Thermal conductivity is the only physical property that shows any remarkable changes with regard to changes in tuff lithology. Relative amounts of sand, silt, and clay were compared with changes in the thermal-conductivity curve, but no correlation was found.

Discussion

The ashy limestones and tuffs sampled in Hole 755A displayed very few changes in physical properties, except in velocity and thermal-conductivity values. The velocity values are about 2600 m/s, with several peaks up to and greater than 4000 m/s. Only one of the velocity peaks (114 mbsf) coincides with a change in lithologic character (to much harder tuff), as compared with the barrel sheets and visual core descriptions. There is a possible correlation between a decrease in the amount of glauconite and decreasing grain density in Subunit IIB. The thermal-conductivity values show some correlation with the tuff lithology character, as discussed previously. High bulk densities and velocities of recrystallized calcite nodules recovered near the base of the hole may reflect the physical properties of lithologies located below the drilling target, the "Jersey Turnpike."

SEISMIC STRATIGRAPHY

Site 755

Site 755 is approximately 4 km north of the prominent southern escarpment of Broken Ridge (Fig. 2). The position of Site 755 was moved approximately 2 km farther south from proposed Site BR-4 to sample lower in the dipping and truncated limestone, chalk, and tuff sequence. Seismic correlation with DSDP Site 255 indicated that this limestone, chalk, and tuff sequence is pre-Santonian in age at Site 755. Another objective of

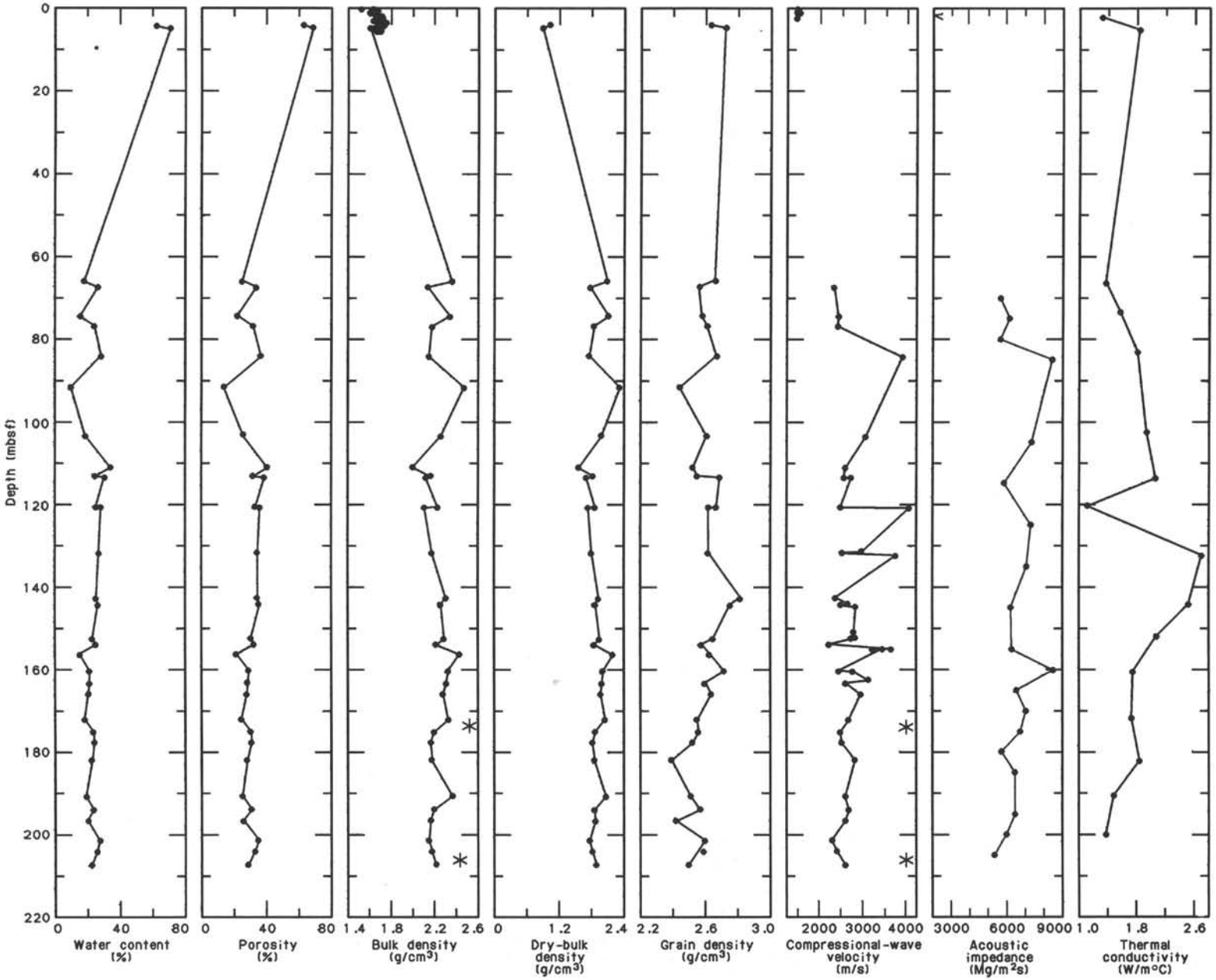

Figure 14. Water content, porosity, bulk density (GRAPE densities plotted as small dots), dry-bulk density, grain density, compressional-wave velocity (P-wave-logger data plotted as small dots), acoustic impedance, and thermal conductivity of sediments from Hole 755A. The interval between 5 and 66 mbsf was not sampled. The low thermal-conductivity value at 121 mbsf is suspect (see text). Stars plotted in the bulk-density and velocity columns are from recrystallized calcite nodules.

Table 9. Compressional-wave velocity of discrete sediment samples from Hole 755A.

Core, section, interval (cm)	Depth (mbsf)	Direction[a]	Compressional-wave velocity (m/s)
5R-2, 93	67.63	A	2338.7
6R-2, 94	74.54	A	2446.7
6R-4, 27	76.87	A	2437.5
7R-2, 114	84.44	A	3917.4
9R-2, 92	103.62	A	3067.6
10R-1, 27	111.17	A	2603.6
10R-2, 121	113.61	A	2566.4
10R-2, 126	113.66	A	2733.3
11R-1, 32	120.82	A	2495.4
11R-1, 52	121.02	A	4067.0
12R-1, 34	131.44	A	2977.9
12R-1, 82	131.92	A	2534.7
12R-1, 143	132.53	A	3758.3
13R-2, 56	142.80	A	2383.5
13R-3, 54	144.14	A	2664.2
13R-3, 79	144.39	A	2502.3
13R-3, 132	144.92	A	2841.9
14R-1, 49	150.89	A	2794.8
14R-2, 41	152.31	A	2829.8
14R-2, 68	152.58	A	2735.4
14R-3, 64	153.97	A	2227.6
14R-4, 18	155.01	A	3454.5
14R-4, 28	155.11	A	3232.0
14R-4, 30	155.13	A	3657.1
14R-4, 32	155.15	A	3452.8
15R-1, 35	160.35	A	2451.8
15R-1, 51	160.51	A	2773.4
15R-2, 104	162.49	A	3144.3
15R-3, 39	163.34	A	2604.1
15R-5, 18	165.96	A	2960.5
16R-2, 99	172.13	A	2677.8
16R-4, 117	175.19	A	2489.0
16R-5, 46	176.16	A	4117.0
16R-6, 77	177.68	A	2524.0
17R-2, 115	181.93	A	2820.9
18R-2, 121	190.81	A	2600.7
18R-4, 140	194.00	A	2676.5
18R-6, 106	196.66	A	2603.4
19R-2, 124	201.44	A	2297.8
19R-4, 87	204.07	A	2410.3
19R-6, 103	207.23	A	2607.7
19R-7, 16	207.86	A	4128.0

[a] A = vertical propagation; B = propagation perpendicular to the split-core face; C = propagation parallel to the split-core face.

Table 10. Thermal conductivity of sediments from Hole 755A.

Core, section, interval (cm)	Depth (mbsf)	Thermal conductivity (W/m°C)
1R-2, 70	2.20	1.313
1R-4, 70	5.20	1.827
5R-1, 126	66.46	1.370
6R-1, 135	73.45	1.570
7R-1, 133	83.13	1.810
9R-1, 137	102.57	1.940
10R-2, 132	113.72	2.060
[a]11R-1, 7	120.57	1.120
12R-1, 139	132.49	2.700
13R-3, 57	144.17	2.520
14R-1, 144	151.84	2.080
15R-1, 54	160.54	1.750
16R-2, 66	171.80	1.730
17R-2, 125	182.03	1.840
18R-2, 98	190.58	1.490
19R-1, 141	200.11	1.380

Note: The interval between 5.20 and 66.46 mbsf was not sampled.
[a] Suspect value (see text).

Site 755 was to recover and determine the lithology that corresponds to the high-amplitude reflector that outcrops at the crest of Broken Ridge (Fig. 15). A suspected talus deposit apparent in both the 3.5-kHz precision depth recorder (PDR) record (30 mbsf, at 1905 hr UTC on 9 May 1988 in Fig. 16) and the water gun seismic-reflection profile north of the outcropping crest of Broken Ridge precluded moving the site any farther south because of the increased risk of hazardous hole conditions (Figs. 16 and 17).

Correlation between Seismic Stratigraphy and Lithostratigraphy

Although continuous downhole sonic and density measurements (i.e., logging) were not conducted at Site 755, discrete compressional-wave and density measurements on samples from Cores 121-755A-1R to 121-755A-19R (0–208.4 mbsf) were used to calculate the velocity and bulk-density data (Fig. 14, "Physical Properties" section, this chapter). The calculated velocities are in good agreement with the velocities derived from sonobuoy solutions for the pelagic cap, lithologic Unit I (Fig. 18). However, the laboratory-measured downcore compressional-wave measurements for Unit II are significantly lower than those derived from the sonobuoys (Figs. 14 and 18). These low-velocity zones are detected in the laboratory compressional-wave measurements, but are not apparent in the sonobuoy data. Several high-velocity intervals are interspersed (e.g., 4100 m/s at 121, 176, and 208 mbsf; see "Physical Properties" section) within the low-velocity zones. Sonobuoy velocity solutions and laboratory downcore compressional-wave measurements indicate average velocities of 1600 m/s for lithologic Unit I (Figs. 14 and 18), and laboratory downcore compressional-wave measurements indicate an average velocity of 2850 m/s for lithologic Unit II (Fig. 14).

Acoustic impedance is the product of velocity and bulk density. Seismic reflectors arise from changes in acoustic impedance with depth. Accordingly, downcore acoustic impedance calculations in conjunction with the seismic velocity allow the correlation of the sampled lithostratigraphy at Site 755 with the seismic stratigraphy. Although major changes in acoustic impedance are noted (Fig. 14), the correlation with observed seismic reflectors is poor (Figs. 16 and 17).

Pelagic Cap

The Neogene pelagic cap, lithologic Unit I, rests unconformably on the Cretaceous and Paleogene dipping and truncated limestone, chalk, and tuff sequence (Fig. 15). Unit I onlaps the truncated and northward-dipping units and probably was deposited under the influence of both currents and relative sea-level changes. The depocenter for Unit I is less than 10 km to the north of Site 755 and was sampled at Site 754. The following reflectors are observed within the horizontal cap:

1. The reflector that coincides with the base of an upper Miocene maximum in the mean grain size of the bulk sediment ("Lithostratigraphy and Sedimentology" sections in the chapters for Sites 752 through 754) at Sites 754, 753, and 752 changes into a fuzzy zone approximately 5 km north of Site 755 (30 mbsf), prior to completely fading out just north of Site 755 (Figs. 16 and 17).
2. The deeper reflector that coincides with an increase in the mean grain size of the bulk sediment within the middle Miocene (~15–16 Ma) at Sites 754, 753, and 752 onlaps the dipping and truncated limestone, chalk, and tuff sequence north of Site 755 (Figs. 16 and 17).
3. The first reflector, at 0.080 s TWT bsf (Figs. 16 and 17) is correlated with a hiatus separating shelly foraminifer grainstone from underlying upper Santonian ashy limestone between Sec-

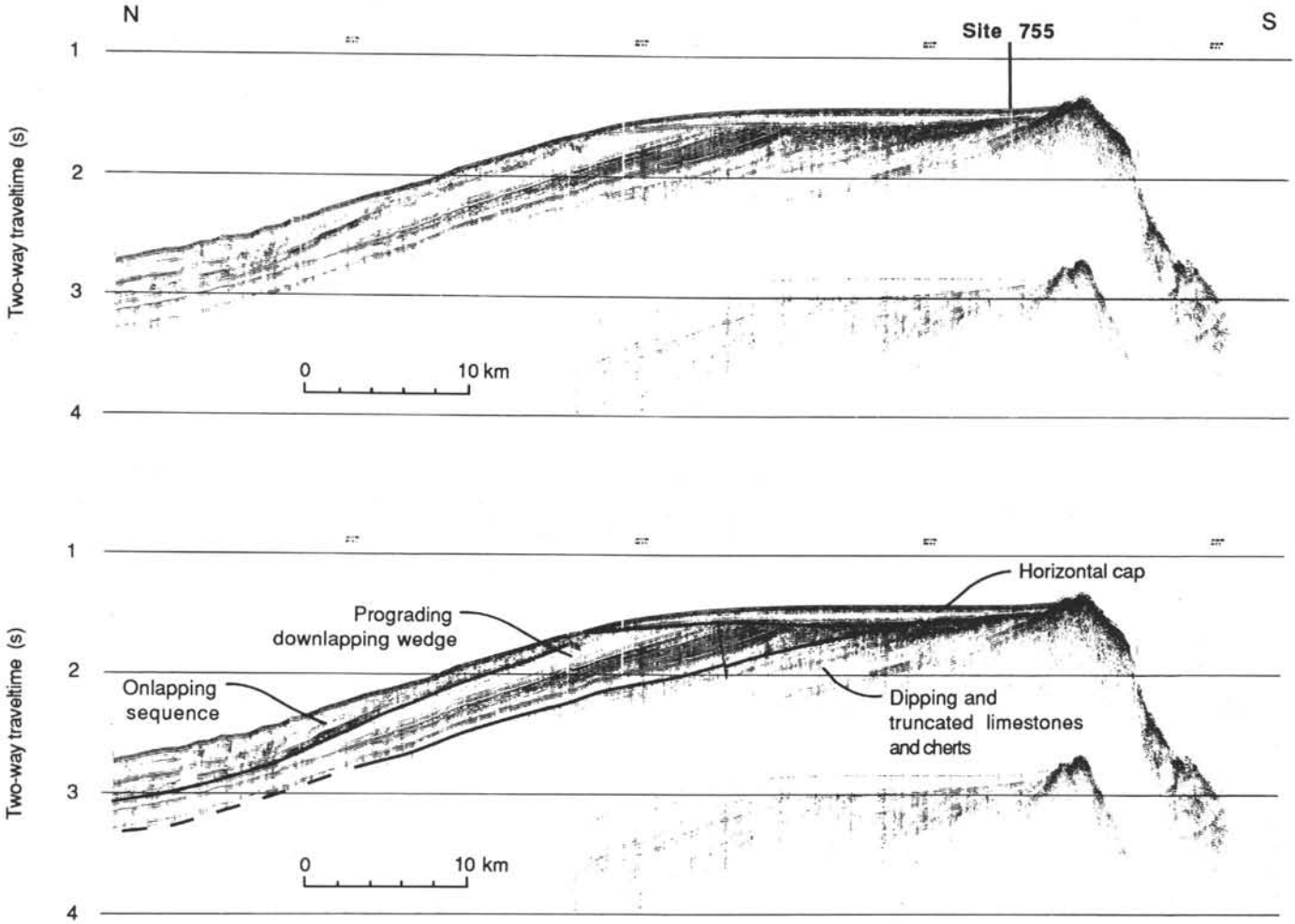

Figure 15. RC2708 single-channel seismic dip line 20 across Broken Ridge, illustrating the stratigraphy observed on and surrounding the ridge. Drilling at Site 755 penetrated the Neogene pelagic cap and bottomed in the dipping and truncated tuff sequence.

tions 121-755A-5R-1 and 121-755A-5R-2. Although there is a paucity of physical-properties data for this interval because of the poor core recovery (Fig. 14), an observable shift in the laboratory-derived acoustic impedance coincides with this angular unconformity at Sites 752, 753, and 754 (see "Physical Properties" sections in the respective site chapters). Seismic correlation with Sites 752, 753, and 754 suggests that a marked change in acoustic impedance should occur at Site 755 (65 mbsf), thereby resulting in this reflector.

Dipping and Truncated Sequences

The dipping and truncated ashy limestone and tuff sequences (seismic stratigraphic limestone and chert sequence) underlying the angular unconformity appear conformable with the pre-existing strata (Fig. 15). The one reflector observed within this sequence, at 0.160 s TWT bsf in the water gun seismic-reflection profile (Fig. 17), correlates with a lithologic change from tuff with varying amounts of glauconite (lithologic Subunit IIB) to a tuff with varying amounts of micrite (lithologic Subunit IIC) between Cores 121-755A-17R and 121-755A-18R. However, there is no corresponding change in the laboratory-derived acoustic impedance at this interval (186 mbsf) (Fig. 14).

Hole 755A was terminated at 208.4 mbsf, prior to penetrating the high-amplitude reflector that outcrops at the crest of Broken Ridge (Fig. 17). Based on the laboratory-derived velocities (see "Physical Properties" sections, this chapter and "Site 754" chapter), approximately 460 m of unsampled sediment exists between the base of Site 754 and the top of the dipping and truncated limestone, chalk, and tuff sequence sampled at Site 755.

REFERENCES

Berggren, W. A., Kent, D. V., Flynn, J. J., and Van Couvering, J. A., 1985. Cenozoic geochronology. *Geol. Soc. Am. Bull.*, 96:1407–1418.

Bolli, H. M., Saunders, J. B., and Perch-Nielsen, K., 1985. *Plankton Stratigraphy*: Cambridge (Cambridge Univ. Press).

Caron, M., 1985. Cretaceous planktic foraminifera. *In* Bolli, H. M., Saunders, J. B., and Perch-Nielsen, K. (Eds.), *Plankton Stratigraphy*: Cambridge (Cambridge Univ. Press), 713–762.

Perch-Nielsen, K., 1985. Cenozoic calcareous nannofossils. *In* Bolli, H. M., Saunders, J. B., and Perch-Nielsen, K. (Eds.), *Plankton Stratigraphy*: Cambridge (Cambridge Univ. Press), 427–455.

Sissingh, W., 1977. Biostratigraphy of Cretaceous calcareous nannoplankton. *In* Haq, B. U. (Ed.), *Nannofossil Biostratigraphy*: Stroudsburg, PA (Hutchinson Ross), 129–144.

Thierstein, H. R., 1974. Calcareous nannoplankton, Leg 26, Deep Sea Drilling Project. *In* Davies, T. A., Luyendyk, B. P., et al., *Init. Repts. DSDP*, 26: Washington (U.S. Govt. Printing Office), 745–771.

_____, 1976. Mesozoic calcareous nannoplankton biostratigraphy of marine sediments. *In* Haq, B. U. (Ed.), *Nannoplankton Biostratigraphy*: Stroudsburg, PA (Hutchinson Ross), 98–128.

Ms 121A-109

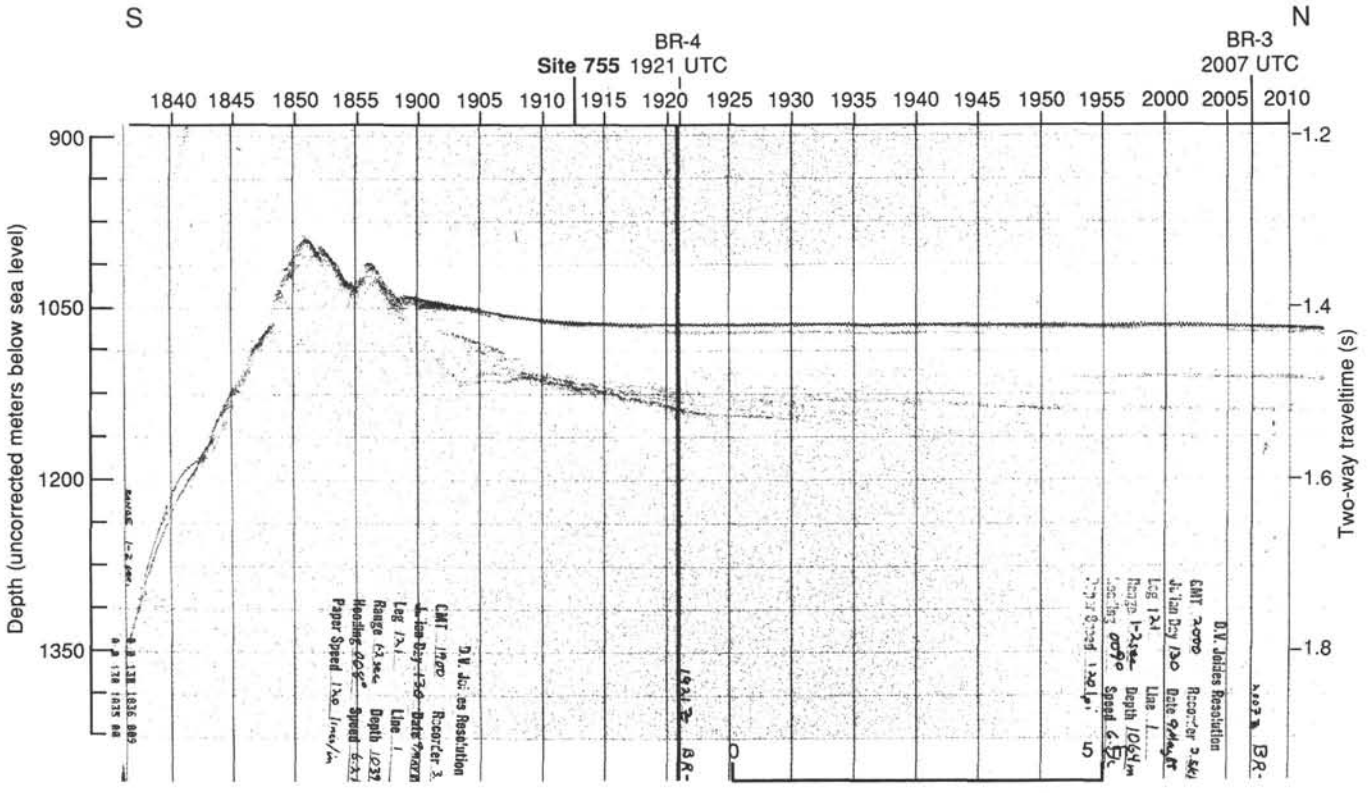

Figure 16. The 3.5-kHz PDR record over Site 755 corresponding to the southern portion of the water gun seismic section shown in Figure 17. The maximum acoustic penetration is approximately 100 mbsf because of the attenuation of the high-frequency signal. The 3.5-kHz profile augments the high-resolution seismic-reflection profile by providing a seismic character for shallow acoustic impedance contrasts that are at or below the vertical resolution of the water gun seismic system.

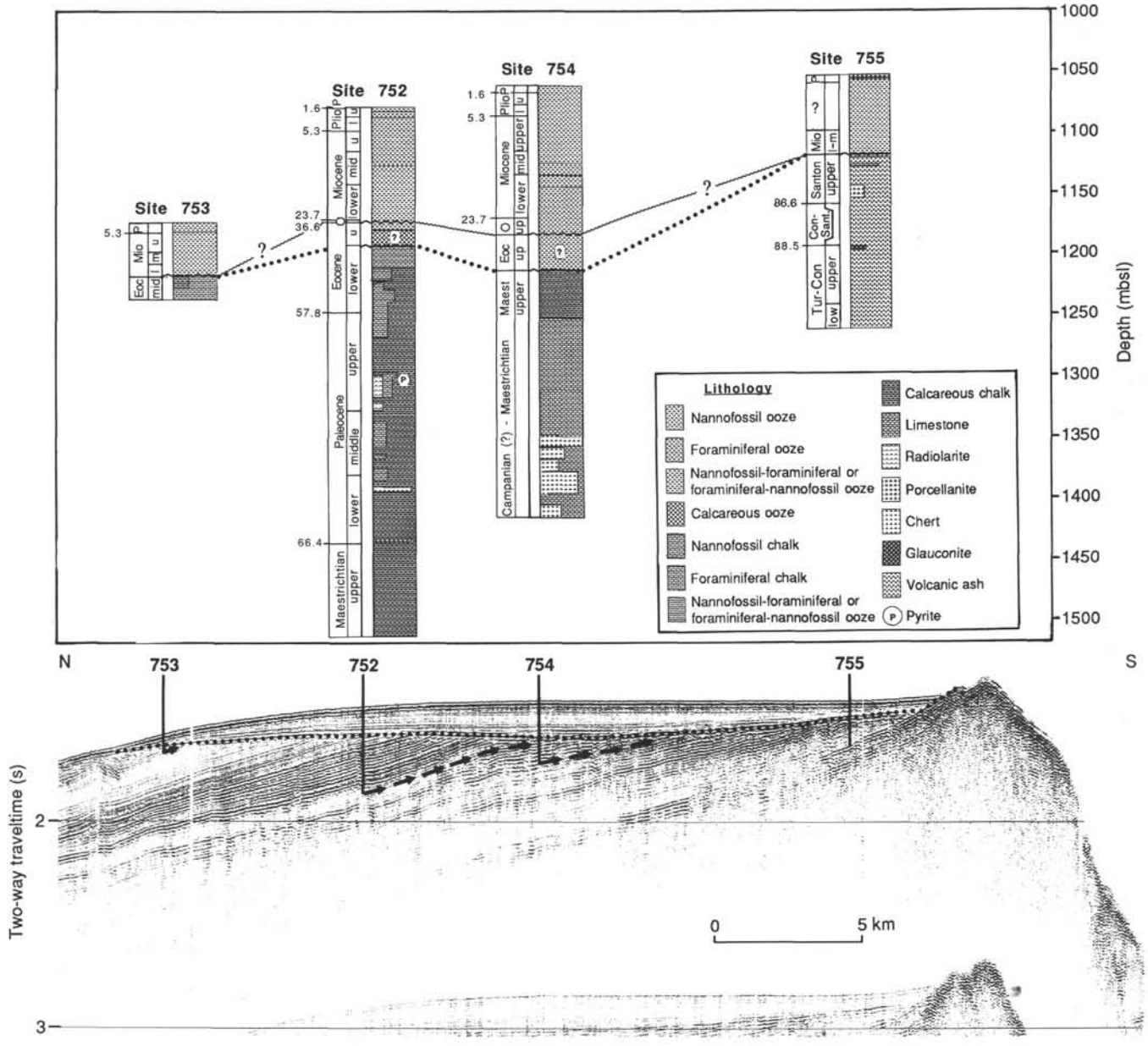

Figure 17. Correlation of seismic stratigraphy and lithostratigraphy sampled at Sites 752, 753, 754, and 755 on Broken Ridge. The arrows represent the continuation updip of the deepest horizon penetrated at Sites 752, 753, and 754 to the angular unconformity, illustrating the amount of stratigraphic section recovered and the stratigraphic overlap—if any—among the sites. The dotted line represents the middle Eocene hiatus and the wavy line denotes the Oligocene hiatus. The two hiatuses coalesce at Sites 753 and 755, but the question marks indicate that the position where they coalesce across Broken Ridge is not resolved.

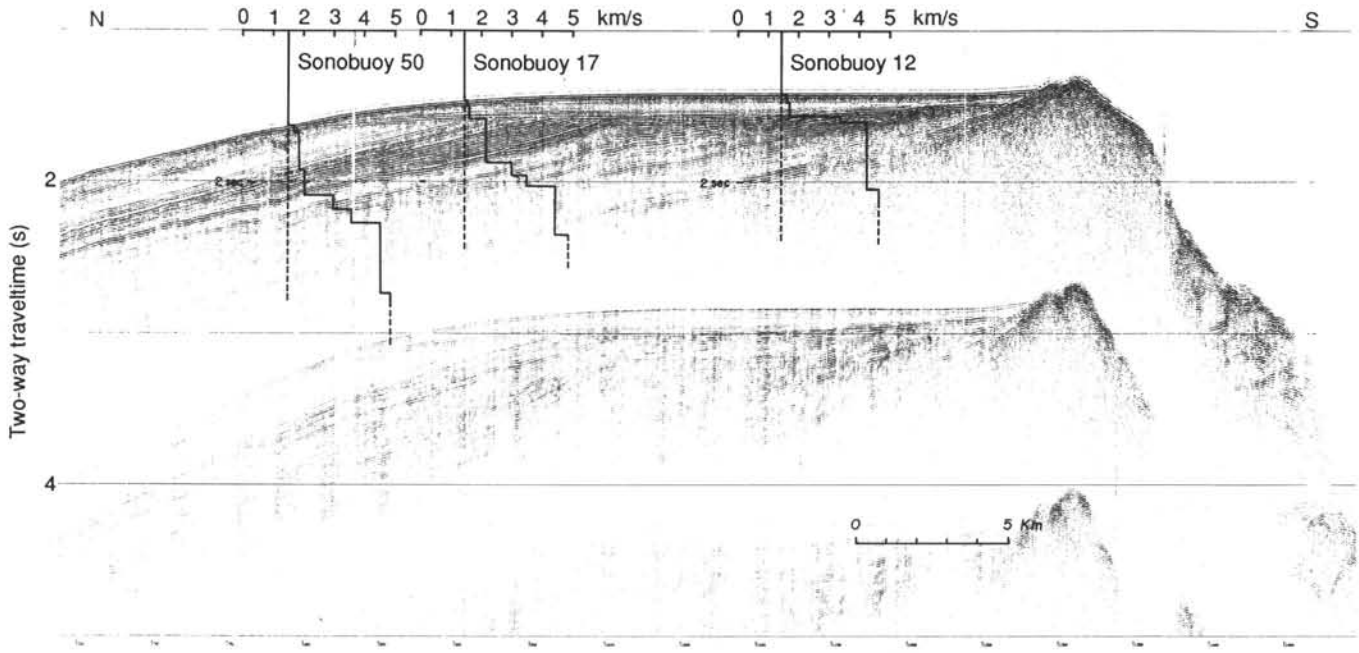

Figure 18. Sonobuoy velocity solutions from strike lines projected onto the dip line, after correcting for changes in water depth. The downsection velocity gradient, from 2200 to 4500 m/s, is also manifested downslope in response to the subcropping reflectors. There is a discrepancy between sonobuoy-derived velocities and laboratory-derived sonic velocities for Site 755.